Marine Geology 477 (2024) 107415

Contents lists available at ScienceDirect

Marine Geology

journal homepage: www.elsevier.com/locate/margo

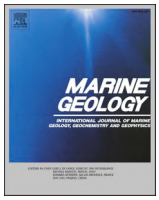

Double tombolo formation by regressive barrier widening and landside submergence: The case of Orbetello, Italy

Gilles Brocard [a,*], Jean-Philippe Goiran [a], Alessandro Conforti [b], Frank Preusser [c], Quentin Vitale [d], Guillaume Jouve [e], Lionel Darras [a], Christophe Benech [a], Cécile Vittori [a], Christine Oberlin [f], Edwige Pons-Branchu [g], Laurent Mattio [e], Arthur de Grauuw [a], Marco Leporati-Persiano [h], Andrea U. De Giorgi [i], Adele Bertini [j]

[a] Archéorient, MOM, UMR 5133, University of Lyon 2, France
[b] CNR, Instituto per lo studio degli Impatti Antropici e Sostenibilità in ambiente marino, 09170 Torregrande, Oristano, Italy
[c] Institute of Earth and Environmental Sciences, University of Freiburg, 79104 Freiburg, Germany
[d] Eveha International, Ivry-sur-Seine, France
[e] Exail, Sonar Systems, La Ciotat, France
[f] Archéologie et Archéométrie, MOM, UMR 5138, CNRS, Université de Lyon 2, France
[g] Laboratoire des Sciences du Climat et de l'Environnement, CEA/CNRS/UVSQ Université Paris-Saclay, Gif-sur-Yvette, France
[h] Lagoon Ecology and Aquaculture Laboratory (LEALab), Orbetello, Italy
[i] National Humanities Center, Department of Classics, Florida State University, 324 Dodd Hall, University Way, Tallahassee, FL 32306, USA
[j] Department di Scienze della Terra, Universitá di Firenze, Italy

ARTICLE INFO

Editor: Michele Rebesco

Keywords:
Double tombolo
Sub-bottom profiles
Orbetello
Tuscany
Regressive sand barrier
Composite tombolo

ABSTRACT

The double tombolo of Orbetello, in Italy, has formed during the Holocene around an ancient central tombolo. Earlier models consider that its sand barriers formed as sand spits that stretched from the mainland to a coastal island before enlarging seawards. This evolution, however, remains speculative. In order to test these models, we conducted the first study of a double tombolo that combines coring of its sand barriers and comprehensive imaging of its internal structure using sub-bottom acoustic surveys offshore and in the back-barrier. Sediment ages were constrained by ^{14}C, luminescence, and U/Th dating. Acoustic images below the lagoon show that the barriers are in fact broad regressive strandplains that initiated on the flanks of the preexisting central isthmus when sea level was -7 ± 1 m lower than today. The strandplains then rose upwards and outwards, tracking sea level rise over the past 7 kyr. The oldest and lowest parts of the strandplains were flooded into the shallow intervening lagoon. The central isthmus is composed of regressive sand barriers accreted around a MIS 5.5 core during subsequent stages MIS 5.3 and MIS 5.1. The emplacement of the isthmus interrupted longshore drift between the mainland and the coastal island, converting the flanks of the initial tombolo into terminal sinks in which sand accretion accelerated, spurring early and rapid regression during the Holocene. A review of the environmental parameters conducive to double tombolo formation suggests that double tombolos may represent a frequent, albeit short-lived stage during the enlargement of single tombolos.

1. Introduction

Tombolos are formed by wave diffraction and refraction in the lee of coastal islands (Farquhar, 1967; Flinn, 1997; Franz et al., 2017; Hsu and Silvester, 1990). Studies of natural tombolo development have investigated the role played by island size, island distance to the mainland, wave climate directionality, and sediment supply, among other variables (Klein et al., 2002; Knight and Burningham, 2022; Sanderson and Eliot, 1996; Sunamura and Mizuno, 1987; Tsuguo, 1987). Double tombolos are much less common than single tombolos, and also much less studied. Their formation has been attributed to the convergence of sand under strongly different wave incidence angles on either side of coastal islands (Blanc, 1982; Gosseaume, 1973). We present here the first comprehensive study of a double tombolo formation combining

* Corresponding author.
E-mail address: gilles.brocard@mom.fr (G. Brocard).

https://doi.org/10.1016/j.margeo.2024.107415
Received 8 May 2024; Received in revised form 11 October 2024; Accepted 16 October 2024
Available online 18 October 2024

sand barrier coring to the sub-bottom imaging of its shoreface and back-barrier. These data allow us to test earlier models of double tombolo formation, which are largely inspired by the way single tombolos develop. The study area is the tombolo of Orbetello, in Tuscany, Italy (Fig. 1A1), which is one of the largest double tombolos of the Mediterranean Sea, together with those of Giens in southern France, and Akrotiri in Cyprus. Unlike these latter, the tombolo of Orbetello also possesses a third, central tombolo, interpreted as an initial single tombolo which growth was superseded by the development of the outer, double tombolo. The three tombolos could have formed in rapid succession after the last glaciation (Ferri and Pranzini, 2006), but the advanced state of diagenesis of the central tombolo suggests instead that it formed during the last interglacial (Coltorti and Ravani, 2017; D'Orefice et al., 2022; Mazzini et al., 1999). The sand barriers of the outer double tombolo are believed to have developed as sand spits after the last glaciation, at some distance from the central tombolo, nucleating at the mainland coast before expanding seawards toward the coastal island of Monte Argentario (Coltorti and Ravani, 2017; D'Orefice et al., 2022;

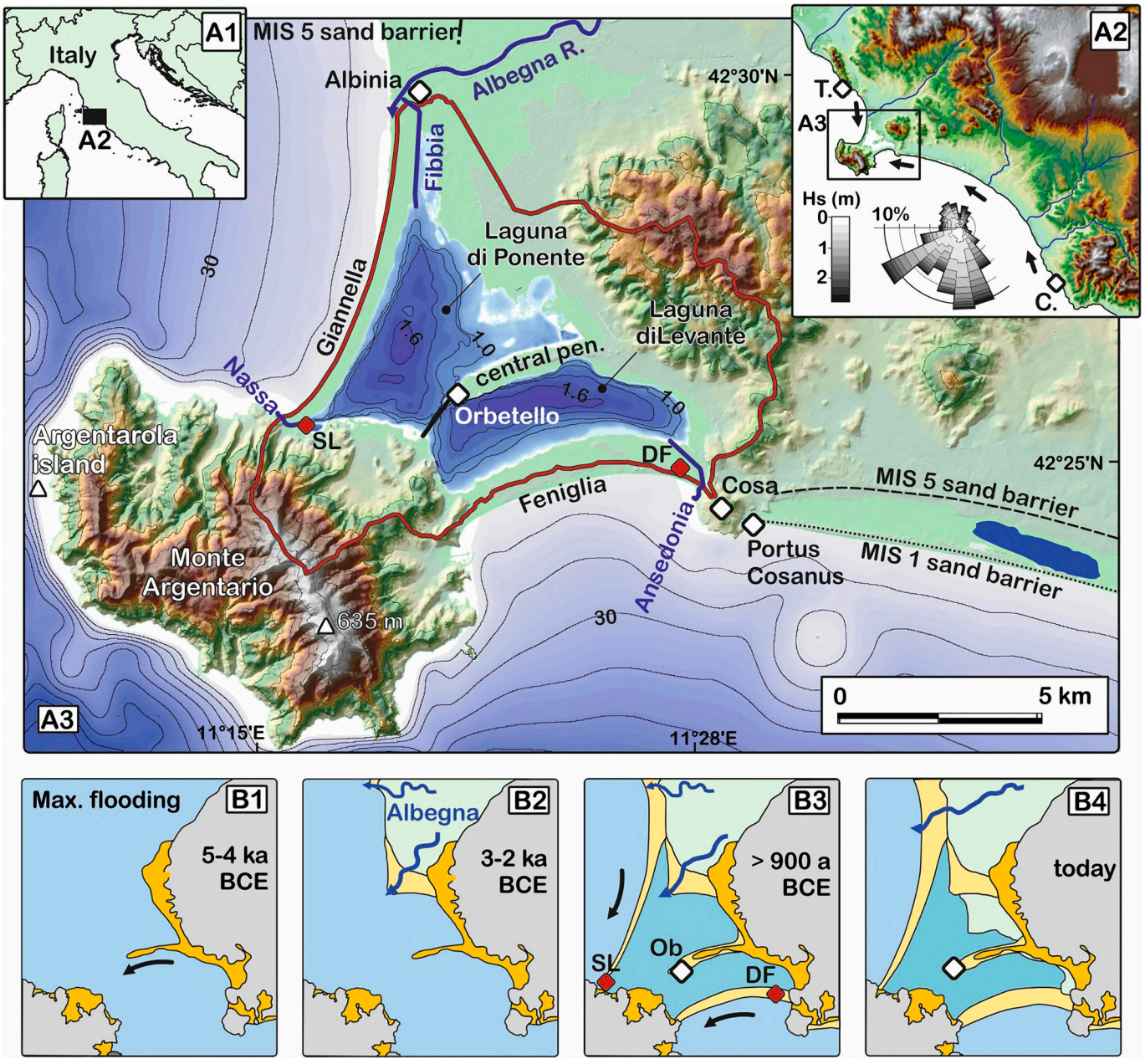

Fig. 1. Geographic setting and earlier models of evolution of the promontory of Monte Argentario. Insets: A1 and A2: location of the study area in Italy (A1), and Tuscany (A2), showing longshore drift directions (arrows), and a rose diagram of the yearly distribution of incoming waves (in % of time) as a function of significant wave height (Hs). Data from MEDATLAS, tile 42N11E (MEDAR_Group, 2002). C and T: towns of Civitavecchia and Talamone. A3: topography and main features. Red line: watershed of the lagoon of Orbetello. Blue lines: canals connecting the lagoon to the sea and rivers. White diamonds: Etruscan-Roman settlements (Ob: Orbetello). Red diamonds: Late Bronze Age settlements (DF: Duna Feniglia; SL: Santa Liberata). Contour line values in meter. Lagoon bathymetry digitized from Cappietti et al. (2006). Onshore topography: 10 m-resolution DTM (CC-BY, Regione Toscana). For colour scale see Fig. 2. Bathymetry: GMRT grid version 11.4, CC BY (Ryan et al., 2009) extracted using GeoMapApp (www.geomapapp.org) CC-BY. Panels B1-B4: paleogeographic evolution, combining key elements of the models by Coltorti and Ravani (2017) and D'Orefice et al. (2022). B1: maximum Holocene flooding. B2: growth of the Albegna River delta in open marine environment. B3: growth of the Holocene sand barriers before the Late Bronze Age. B4: final closure of the lagoon. (For interpretation of the references to colour in this figure legend, the reader is referred to the web version of this article.)

Ferri and Pranzini, 2006). In doing so, the two sand spits progressively enclosed a large intervening lagoon, in which lies the central peninsula. The city of Orbetello was settled on this peninsula by the Etruscans in the 8th century BCE (Fig. 1B). Today, the lagoon is very shallow (≤1.7 m deep) and artificially connected to the sea and to a nearby river (the Albegna River) by a series of manmade canals (Fig. 1A3). Shallow depth and limited connection to the sea make the lagoon highly sensitive to eutrophication. Since the second half of the 20th century, land fertilizers, industrial phosphate processing, fish farming and urban development have triggered acute chronic eutrophication crises, motivating numerous environmental studies, large remediation operations, and costly maintenance (Cappietti et al., 2020; Cioffi and Gallerano, 2001; Lenzi et al., 2003). Over the years, the sustainability of such operations have been questioned, as well as the actual contribution of anthropogenic activities to eutrophication. Indeed, shallow depth and chronic eutrophication are expected in a lagoon that has reached its final stage of siltation, in line with the evolution of nearby lagoons along the coast of Tuscany (Bellotti et al., 2004; D'Orefice et al., 2020). In order to address whether eutrophication is natural and irreversible, it is important to understand the evolution of its enclosing double tombolo.

We cored and dated by radiocarbon, luminescence, and U/Th dating the three tombolos of Orbetello to document their growth pattern. We acquired acoustic profiles at 3.5 kHz offshore and at 10 kHz in the lagoon to reveal their sedimentary architecture and stratigraphic relationship with back-barrier layers. These datasets lead us to propose an alternate model of double tombolo development which radically differs from earlier models.

After reviewing previous chronological constraints on the formation of these tombolos, we introduce the methods used in this study and present their most salient results. We then discuss their implications relative to the formation of the triple tombolo, by focusing successively on: 1) the growth pattern of the double tombolo, 2) the mode of emplacement of the intervening lagoon, 3) the formation of the central peninsula, 4) its reshaping during the last glaciation, and 5), in light of the previous elements, we discuss the environmental variables conducive to double tombolo formation.

2. Regional setting

The headland of Orbetello-Monte Argentario is a promontory located on the coast of Tuscany that juts out 15 km into the sea (Fig. 1A2). Its is composed of the former island of Monte Argentario, which is 10.5 km long, 7.3 km wide, and 635 m high, that used to lie 4–5 km offshore, and of the *Tombolo della Giannella* in the north, and *Tombolo di Feniglia* in the south that nowadays connect it to the mainland. These two tombolos are hereafter referred to as the Giannella sand barrier (Giannella SB) and Feniglia sand barrier (Feniglia SB). The Giannella SB is 9 km long and rises 7 m above modern sea level. It is 0.65 km wide at its northern end where it connects to the mainland and narrows down to 0.30 km at its southwest end, at the foot of Monte Argentario (Fig. 2B). The Feniglia SB is 6 km long and culminates at 14 m above sea level. It is 0.80 km wide at its mainland end, narrowing down to 0.65 km at the foot of Monte Argentario (Fig. 2C). The two barriers enclose the vast (27.3 km^2) and shallow (≤ 1.7 m deep, average depth 1.04 m) *Laguna di Orbetello* lagoon. The latter is divided into two subbasins of roughly equal size and depth by the 13 m-high, 3.5 km-long, and 0.55 km-wide peninsula of Orbetello, which is attached to the mainland at its eastern end. Its western end is buried under the lagoon over a distance of 1 km. It separates the *Laguna di Levante* subbasin in the southeast from the *Laguna di Ponente* subbasin in the northwest (Fig. 1A3). The central peninsula was settled by Etruscans in the 8th century BCE (Perkins, 2010). The city of Orbetello was surrounded by defensive walls (Fig. 2D) during Antiquity, long believed to have been built during the 6th century BCE (McCann, 2017) but recently assigned to the 3rd century BCE (Campioltrini, 2019), the settlement phasing out shortly thereafter (De Giorgi, 2023). The city has been regarded as a lively Etruscan harbor (Michetti, 2017; Pincherle and Volpi, 1989) at a time when the lagoon was presumably accessed from the sea via a natural or, more likely, an artificial waterway (Negroni Catacchio et al., 2017). It stands to reason that the fortunes and recession of ancient Orbetello were predicated on the conditions of the lagoon at any given point in time.

The tidal range around Orbetello only reaches 0.45 m (Ferrarin et al., 2013). As a result, onshore sediment transport is mostly influenced by wave climate. The general circulation of surface seawater in the Tyrrhenian Sea is characterized by a counter-clockwise gyre that generates northwestward drift along the Italian Peninsula (Vetrano et al., 2010). In the northern part of the Tyrrhenian Sea, where Orbetello is located, the largest and most frequent waves track from the south and southwest (Fig. 1A2), with a dominance of southwest-tracking waves in winter (MEDAR_Group, 2002). This wave climate generates an overall SE–NW–oriented drift along the entire stretch of coast, disturbed locally by promontories such as Orbetello, down-drift of which return clockwise gyres are formed (Cutroneo et al., 2017). The promontory of Orbetello-Monte Argentario thus constitutes the boundary between two converging coastal cells: a major southern cell that conveys sand to the NW, bound to the south by the headland of Civitavecchia (Capo Linaro), 60 km south of Orbetello (Fig. 1A2), and a shorter, opposite northern cell, bound to the north by the cape of Talamone, 13 km north of Orbetello (Fig. 1A2). The Feniglia SB constitutes the terminal sink for beach and shoreface sands tracking from the south (Pranzini et al., 2020). It is rich in volcanic minerals (Bartolini et al., 1977) derived from the Middle Pleistocene Roman volcanic province (Pranzini et al., 2020), widely spread across the southern shelf (Tortora, 1989). Likewise, the Giannella SB constitutes the terminal sink for sands transported southwards along the Giannella SB (Gosseaume, 1973), provided mostly by the Albegna River (Ferri and Pranzini, 2006).

The degree of induration of the central peninsula is comparable to that of nearby Tyrrhenian (MIS 5.5) sand barriers found at similar elevations (Nisi et al., 2003). Induration motivated its ascription to the last interglacial (D'Orefice et al., 2022; Mazzini et al., 1999). The Giannella and Feniglia sand barriers, on the other hand, are not indurated and would have formed during the Holocene (Fig. 1B1-4), growing initially as sand spits from the mainland toward Monte Argentario, before broadening on their sea side (Coltorti and Ravani, 2017; D'Orefice et al., 2022). A scarp (Fig. 2D) that runs along the southern flank of the central peninsula has been interpreted as an erosional cliff, etched during the maximum of the Holocene transgression before the sand barriers were emplaced (Coltorti and Ravani, 2017). The lagoon of Orbetello would have formed by progressive isolation from the sea behind the developing spits. Freshwater runoff to the lagoon is limited by its modest catchment size (51 km^2 of land area plus 27 km^2 of lagoon). In the west, the catchment includes the east flank of Monte Argentario and, in the east, the west flank of an earlier headland. Runoff is further limited by water infiltration in the Triassic limestones that underlie these areas. Part of the infiltrated water feeds exsurgences outside the catchment (Bianchi et al., 2006). The Albegna River, to the north (Fig. 1A3), is not currently part the natural catchment, but it provides water to the lagoon via the regulatory canal of Fibbia. This canal straddles a lowland which lies low enough for floodwaters from the Albegna River to spill into the lagoon. Coltorti and Ravani (2017) interpreted the area stretching from the Albegna River to the lagoon of Orbetello as a former delta lobe of the Albegna River into the lagoon. D'Orefice et al. (2022) proposed that this purported delta owes its cuspate shape to its exposure to sea waves before the Giannella SB sheltered the delta from the sea (Fig. 1B2, 3). The rerouting of the Albegna River to its current outlet, or, alternately, the abandonment of a southern distributary channel of the Albegna River, would have subsequently ended the continuous inflow of freshwater and sediment from the Albegna River into the lagoon. Such rerouting/abandonment would have occurred either naturally, before Antiquity, or artificially, during Antiquity (Coltorti and Ravani, 2017). The remains of a fluvial Roman harbor on the river banks at Albinia (Fig. 1A3), 400 m upstream of the river mouth, provide a minimum age

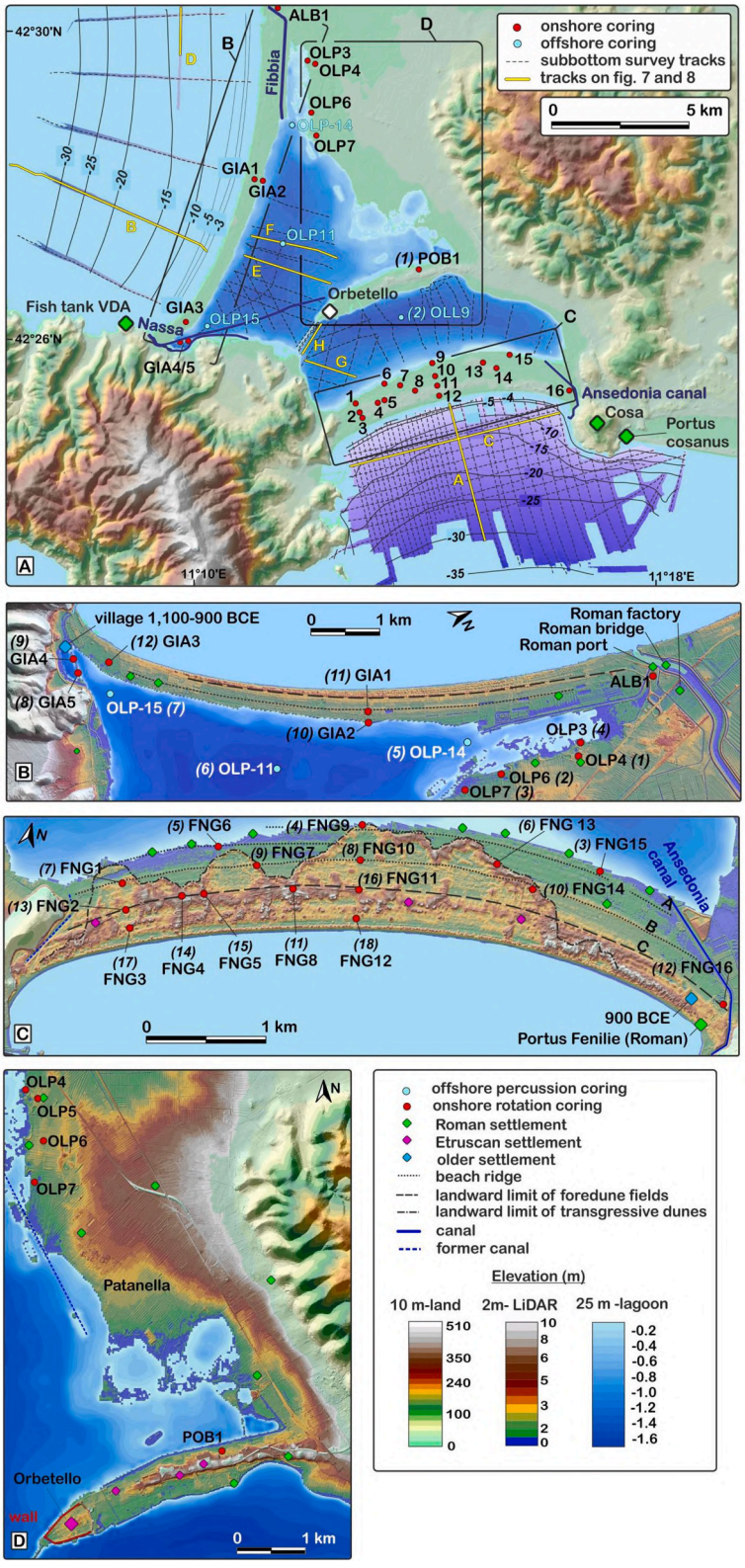

Fig. 2. Coring and sub-bottom profile locations. (A) general map of Orbetello. VDA: Fish tank of Villa Domitius Ahenobarbus. Land topography: 10 m-resolution DTM (CC-BY, Regione Toscana). Offshore bathymetry: 10 m-resolution DEM (Brocard and Conforti, 2023), with contour lines every 5 m below −5 m, and every 1 m above −5 m. Lagoon bathymetry digitized from Cappietti et al. (2006). B: topography of the Giannella sand barrier, C: topography of the Feniglia sand barrier. D: topography of the central peninsula and of the Patanella area. Land topography on B, C, and D: 2 m-resolution LiDAR DTM (Ministero della Transizione Ecologica CC BY 3.0). Ancient settlement locations from (Dolci, 2014; Negroni Catacchio et al., 2019). Bracketed numbers in italic: core order as displayed on the transects of Figs. 4 and 5.

of 2 ka for the current course of the Albegna River. A core extracted nearby (ALB1, Fig. 2A3) further indicates that the delta plain had reached the Giannella sand barrier by 4.7 ka (Chapkanski et al., 2021). Bronze and early Iron Age settlements (2.9–3.1 ka) excavated on the sand barriers indicate that the sand barriers already fully enclosed the lagoon before Antiquity (Bartolini et al., 1977; Dolfini, 2017; Schmiedt, 1972). The strongest evidence comes from a Late Bronze-Early Iron Age (2.9–3.1 ka) village settled at Santa Liberata on the Giannella SB, where the barrier abuts Monte Argentario (Poesini, 2012). Likewise, a 2.9 ka settlement (Duna Feniglia, DF, Fig. 1A3) has been excavated on the eastern end of the Feniglia SB (Rossi, 2017; Rossi et al., 2014). Etruscan artefacts (2.8–2.3 ka) scattered along the Feniglia SB (Negroni Catacchio et al., 2019) further suggest that the Feniglia SB was then emerged over its entire length, behind a seashore located no more than 230 m inland from the current shore. Ruins of Roman naval facilities near the site of Duna Feniglia (Portus Fenilie, in the medieval tradition) further indicate that, by Roman times, the same seashore lied within 60 m of its current location.

3. Materials and methods

3.1. Coring

3.1.1. Terrestrial coring

We conducted extensive coring around the lagoon in order to 1st, map the extent and thickness of the Holocene sand barriers, and 2nd, determine the nature, age, and depth of their substrate. Twenty-six cores were collected using a track-mounted drill rig, operated by Geoambiente soc. Coop. a.r.l (Fig. 2A, Table S1–1). During drilling operations, a coring barrel was pushed down hole by a flight of drill rods, lowered by rotation using water as cooling and lubrication fluid. Each borehole was cased from top to bottom with a steal liner, lowered by rotation to the depth of the drill bit after each 1 m- to 1.5 m-long coring increment. The cores were extruded from the barrel horizontally using a hydraulic piston, then stored in standard core plastic boxes containing 5 × 1 m of cores, and finally transported to the Archéorient Laboratory storage facility in Jalès, Berrias-Casteljau, France (University of Lyon 2), for detailed logging and sampling.

Core elevations were extracted from the 2 m-resolution LiDAR DTM, kindly provided by the Ministero della Transizione Ecologica CC BY 3.0 (http://www.pcn.minambiente.it).

3.1.2. Lagoonal coring

Cores were collected in the lagoon of Orbetello (Fig. 2A, Table S1–1) from a boat provided by the sailing club of Orbetello using a 6 cm-diameter Uwitec gravity corer with hammer action, by manual down-hole percussion of PVC tubes. Three 1.3 to 2.3 m-long cores (labelled OLP-1×) were collected in the northwestern subbasin (*Laguna di Ponente*). A 1.1 m-long core (OLL-9) was collected in the southeastern subbasin (*Laguna di Levante*). The PVC tubes were opened, photographed, and sampled at the EDYTEM Laboratory, Université de Savoie-Mont Blanc, France, before archiving at the OMEAA storage facility, EVS-Archéorient laboratories, University of Lyon 2, France.

3.2. Dating

3.2.1. Radiocarbon dating

We extracted 34 samples from the cores for radiocarbon dating, among which 12 came from the Giannella barrier, 18 from the Feniglia barrier, and four from the lagoon (Table S2–1). Most sand barrier samples consisted of seagrass fibers, a few of terrestrial plant remains, and one sample was a shell fragment of the marine gastropod *Charonia tritonis*. In the lagoon, dating was conducted on bulk organic-rich clay.

Twenty-five samples were prepared for Accelerated Mass Spectrometry (AMS) at the Centre de Datation par le Radiocarbone of Lyon (ArAr laboratory, University of Lyon 2, France). The samples were measured on the ARTEMIS AMS facility, UMS 2572, at the LMC14 laboratory, Saclay, France, and on the AMS facility from the Centre for Isotope Research (CIO) at the University of Groningen, Netherlands. Seven samples were prepared and measured for radioactive decay counting at the Centre de Datation par le Radiocarbone of Lyon, France. The majority of non-carbonate-containing samples underwent an acid-base-acid pretreatment (ABA). The strength of treatments can vary, depending on the fragility of the material. The ABA pretreatment is designed to remove sedimentary carbonates, humic and fulvic acids, and dissolved atmospheric carbon dioxide that may have been absorbed during the base wash. Each acid or base wash is followed by rinses with ultrapure deionized water.

The standard pretreatment method for shells involves surface cleaning by air abrasion with aluminum oxide powder to remove the outer surface and rinsing with ultrapure water, using ultrasonication if required, to clean the shell. Samples are then dried and roughly crushed. If necessary, the surface of the shells is acid-etched with 0.1 M hydrochloric acid.

Calibrated calendar ages (Table S2–1) were computed using the online software Oxcal v. 4.4 (https://c14.arch.ox.ac.uk/oxcal.html). Terrestrial plant fragments were calibrated using the continental calibration curve of Reimer et al. (2020). Marine organisms were calibrated using the marine calibration curve of Heaton et al. (2020), which includes a time-varying global marine reservoir age which, over the dated period, fluctuates between 300 and 500 years, assuming negligible systematic integrated local reservoir age departure ($\Delta R = 0$) in the study area (Reimer and McCormac, 2002). Bulk sediment ages from the lagoon were calculated considering the possibility of both a marine and continental origin for the bulk organic matter. In the absence of ΔR values for the lagoon, these marine calibrations are regarded as minimum limiting ages, as reservoir effects in Mediterranean lagoons tend to be larger (Sabatier et al., 2010; Zoppi et al., 2001) than the global marine reservoir age of ~450–550 years (Heaton et al., 2020). Note that ages are reported on figures within their 95% probability interval (Table S2-1) as #±# ka for visualization purpose, as calibrated probability distributions are actually complex composite normal distributions.

3.2.2. $^{230}Th/^{234}U$ dating

In core GIA-1, the substrate of the Giannella SB is composed of partially cemented, shell-rich and organic-rich marine sands. A coral from this substrate (GIA1–1363, Table S3–1) was collected and dated by $^{230}Th/^{234}U$ dating at the Laboratoire des Sciences du Climat et de l'Environnement (LSCE, France). The sample was mechanically cleaned using a Dremel diamond wheel. ~ 20 mg were extracted and dissolved in a PTFE beaker, to which a known amount of ^{229}Th-^{236}U-^{233}U spike had been previously added. Uranium and thorium were then co-precipitated with $Fe(OH)_3$, which was digested in nitric acid. They were then purified and separated on ion exchange columns using U-TEVA® resin. The isotopic composition of the uranium and thorium separates was analyzed on a Multi-Collector Inductively Coupled Plasma source Mass Spectrometer (MC-ICPMS) Thermo Scientific™ NeptunePlus, fitted with an Aridus II™ introduction system. The detailed procedure (chemistry and MC-ICPMS analysis) is detailed in (Pons-Branchu et al., 2022); Pons-Branchu et al. (2014). After corrections for mass fractionation, peak tailing, hydrate interference and chemical blanks, $^{230}Th/^{234}U$ ages were calculated from the isotopic ratios through iterative age estimation using the ^{230}Th, ^{234}U and ^{238}U decay constants of Cheng et al. (2013), and Jaffey et al. (1971).

3.2.3. Luminescence dating

15 core samples were collected for luminescence dating (Table S4–1), including 10 samples from the Giannella SB (GIA1, 2), one from the Feniglia SB (FNG9), three from the northern lowland (Patanella, OLP3, 7), and one from the central peninsula of Orbetello (POB1). Samples were processed at the luminescence dating laboratories of the University of Freiburg (Germany) by first gaining the grain fraction

100–250 μm by wet sieving. Using a large grain size range was required due to the limited diameter of the core samples. After chemical pre-treatments (HCl, H_2O_2, Na-oxalate), a K-feldspar and a quartz fraction were isolated by two-step heavy liquid density separation ($\delta = 2.58$ g cm^{-3} and $\delta = 2.70$ g cm^{-3}, respectively). The latter separate was etched for 60 min in 40 % HF, followed by 10 % HCl treatment. Measurements were done on a Freiberg Instruments Smart device (Richter et al., 2013), calibrated using LexCal 2014. For equivalent dose (D_e) of quartz (2 mm aliquots), a modified version of the single aliquot regenerative dose protocol (Murray and Wintle, 2000) was used with the preheat set to 230 °C prior to measurement of the optically stimulated luminescence (OSL) signal (beta dose rate of source in device = 0.123 Gy s^{-1}). For samples with a D_e of >50 Gy, the multi-elevated temperature post-IR infrared stimulated protocol (here abbreviated as pIR) of Li and Li (2011) was used for D_e determination of feldspar (dose rate = 0.633 Gy s^{-1} after installation of new source), using the stimulation at 200 °C for age calculation (Schulze et al., 2022; Schwahn et al., 2023). Depending on the observed overdispersion and shape of D_e distributions, appropriate models were selected to calculate average D_e of the samples (Galbraith and Roberts, 2012). The concentration of dose-rate relevant elements (K, Th, U) was determined by low-level gamma spectrometry (at VKTA Rossendorf e.V.). The ADELE software was used for age calculations (www.add-ideas.com), assuming samples have been water saturated all time (37 % moisture content). An internal K-content of 12.5 ± 0.5 % (Huntley and Baril, 1997) and an a-value of 0.07 ± 0.02 were used for feldspar. Cosmic dose rate was calculated using corrections for geographic position and depth (Prescott and Hutton, 1994).

3.3. Sub-bottom profiles

3.3.1. Marine 3.5 kHz sub-bottom profiles

Sub-bottom acoustic profiles were acquired offshore (Fig. 2A) in October 2022 by the research vessel Haliotis (French Oceanographic Fleet), operated by Genavir, during the HISOPE cruise (https://campagnes.flotteoceanographique.fr/campagnes/18002090/fr). Acquisition involved an Echoes 3500 T1 (Exail) sub-bottom profiler which produces a 10–50 ms–long chirp signal between 1.7 and 6.2 kHz. It possesses a 15 cm vertical resolving power, and a penetration depth of up to 15 m in such sand-rich environment. Pitch, roll, and heave were recorded by an inertial navigation system (iXsea), corrected in real time using the SUBOP acquisition system (©IFREMER). Ship location was provided by the Orpheon network real-time kinematic positioning (RTK). Data were validated, processed, and replayed using the QC-SUBOP software (©IFREMER). Post-processing resorted to the Geosuite All Works software, which workflow involves signal normalization, basic band pass filtering, and gain adjustment by Liner Gain (LG) or Time Varying Gain (TVG), depending on acquisition depth and sea bottom reflectivity.

3.3.2. Lagoonal 10 kHz sub-bottom profiles

Sub-bottom acoustic profiles were acquired in the lagoon of Orbetello in 2021 and 2022 (Fig. 2A) using a boat provided by the Fishermen of Orbetello cooperative, in water depths ranging from 0.8 to 1.6 m. A 10 kHz pole-mounted Exail sub-bottom profiler (T3 Echoes 10,000) provided a 7.5 cm vertical resolving power and a penetration depth of up to 12 m. Data acquisition was conducted using the Delph Seismic Acquisition software (Exail). Post-processing and interpretation were handled using the Delph Seismic Interpretation software. Data visualization and assembly were performed using the software Delph Roadmap.

4. Results

Sedimentary facies, core stratigraphy, and core correlations are presented in Section 4.1. The radiocarbon, luminescence, and U/Th ages, their consistency, and the resulting core correlations are presented in Section 4.2. The lagoon acoustic profiles were then used to identify lagoon layers, Holocene sand barriers, and Pleistocene basement (Section 4.3). The offshore profiles provided additional constraints on the outer growth of the sand barriers, and on the geometry of their substrate (Section 4.4). Throughout the following result and discussion sections, elevation is provided relative to modern sea level.

4.1. Sedimentary facies associations and depositional environment

The sand barriers are composed of low-angle planar-parallel-stratified sands (Fig. 3). The sands are arranged in alternations of decimeter-thick beds of different facies. Facies 1 consists of quasi-planar laminated couplets, composed of well-sorted medium- to fine-grained sand alternating with thin layers of sandy silt (Fig. 3A). Facies 2 consists of well-sorted medium- to coarse-grained massive sand (Fig. 4D). At places their alternation occurs at the sub-decimeter scale (Fig. 4B). In the couplets of facies 1, sand laminae are thicker than intervening silty sand laminae, the latter maintaining a fairly constant thickness of a few millimeters. Conversely the sand laminae thickness varies substantially, and, at places, steadily increases or decreases along core (Fig. 4A). The coarse massive beds of facies 2 are most commonly isotropic. At places, they exhibit normal grading over a basal scour (Fig. 4D). Facies 1 is more common in the Feniglia SB than in the Giannella SB. In the latter, the coarse sands of facies 2 alternate with a facies 3 which, like facies 1, is composed of well-winnowed medium-to fine-grained sand that are slightly more heterometric. Layering is also fainter in facies 3, which displays discontinuous silty sand laminae that appear disrupted by biodeformation or by bottom currents (Fig. 4C). No cross-bedding is observed anywhere in the successions. The coarsest grains in heterometric sands and at the base of graded beds are bioclasts. Fine-grained facies 1 and 3 are more abundant at the base of the sand barriers, whereas coarse-grained beds dominate up section.

The depth of deposition of these sands can be appraised from their distance to the overlaying sand barrier surface and their current depth (which represents their minimum depth of deposition, assuming constantly rising sea level), and by modern depositional environments along the coast. Currently, along the southern littoral cell, sands and silty sands of the shoreface stretch from the beach down to depths of −10 to −15 m. Farther offshore, the seafloor is covered by finer-grained sandy silt, blanketed by seagrass meadows (Borelli et al., 1986; Tortora, 1989; Tortora, 1996b). Along the Feniglia SB, beach and upper shoreface sediment grain-size is bimodal (sand and very fine silt) to unimodal (sand) (Tortora, 1996b). The median grain size of the sand fraction decreases from 0.21 ± 0.06 mm (1 σ) at the beach, down to 0.15 ± 0.02 mm (1 σ) at −10 m (Bartolini et al., 1977).

Sediment deposition in both sand barriers occurred above a basement which current depth is shallower than 17 m, that is, within the current depositional range of silty sand (Tortora, 1996b). In the cores, this corresponds to the deposition of the laminated silty sands (facies 1 and 3), interrupted by the emplacement of medium to coarse sand sheets (facies 2), which we tentatively interpret as deposits of sandy gravity flow that avalanched from the upper shoreface during storms (Field and Roy, 1984; Flores et al., 2018). In this context, the upward increase in the frequency of coarse sand beds, which is more pronounced in the Giannella than in the Feniglia sand barrier (Figs. 4 and 5), is interpreted as the progressive shoaling of the shoreface during sand barrier progradation. No clear transition to the upper shoreface or beach face is observed, however. Swath bathymetry (Brocard and Conforti, 2023) and earlier bathymetric data (Gisotti and Lembo, 1992) show that, along the Feniglia SB, a 1.5 m-high longshore bar lies 180 m from the shore, its ridgeline as shallow as 2.5–3 m. A sand bar rising within −2.5 m of the surface is also present 180 m off the Giannella SB (Brocard and Conforti, 2023). The absence of cross-stratified sands in the cores, commonly observed in longshore bars, may reflects the fact that bar deposits are rarely found intercalated in shoreface successions (Immenhauser, 2009) where quasi-planar and swaley cross-stratifications dominate (Pemberton et al., 2012). The only unambiguous beach face deposits

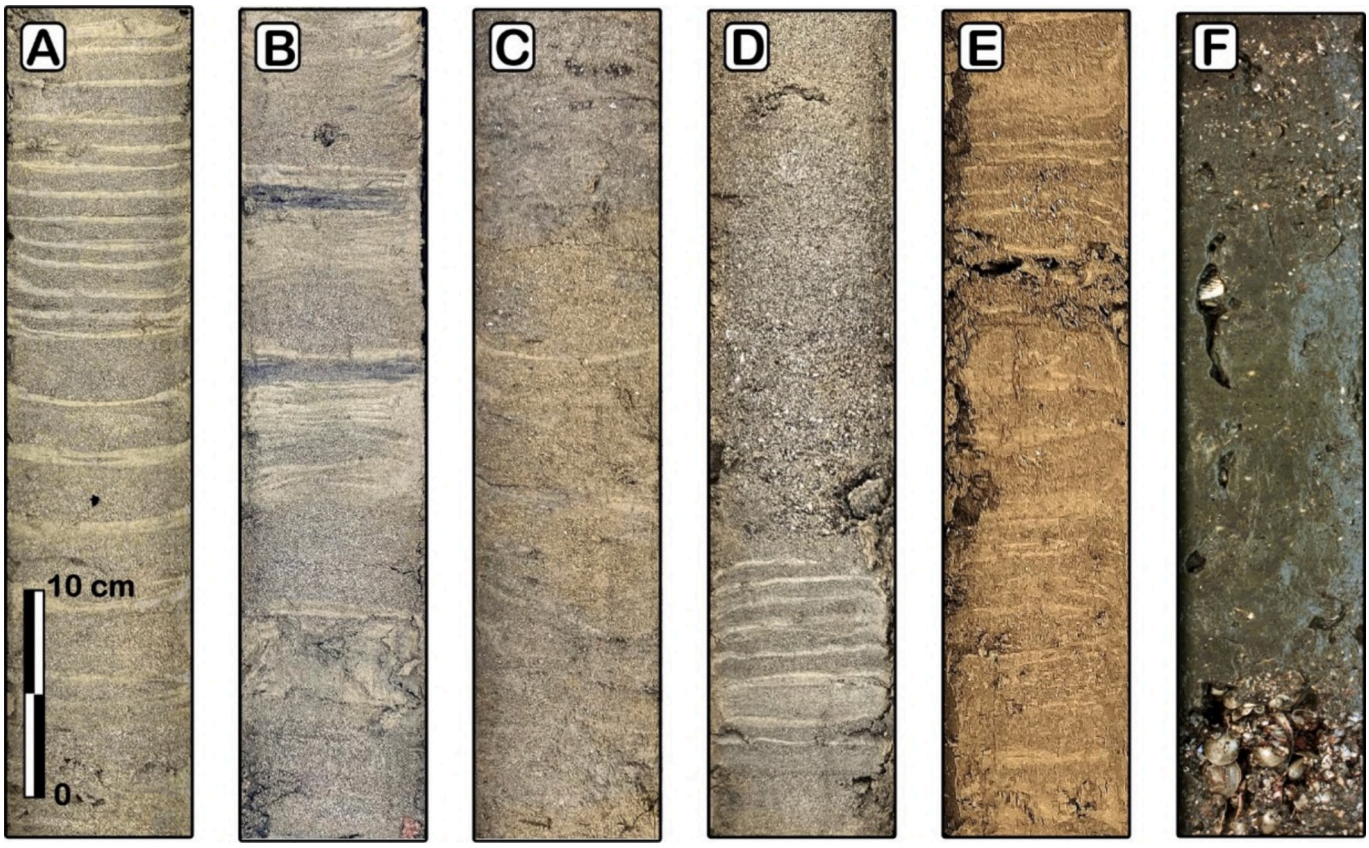

Fig. 3. Photographs showing the most commonly cored facies. A: alternation of sand and silty-clayey sand laminae (facies 1, FNG-11, −8.4 m). B: alternation of laminated silty sand and homogenous medium sand (FNG-10, −3.7 m). C: sands of facies 3 (GIA-3, −8.5 m). D: facies 2: coarse, homogenous, fining-upward sand with basal unconformity over laminated alternations of fine sand and silty sand of facies 1 (FNG-9, −10.1 m). E: Pleistocene marine sand, facies similar to facies 1 (FNG-9, −21.2 m). F: Holocene lagoonal, organic rich, shelly sapropel with coquina levels (OLP-15, −1.5 m).

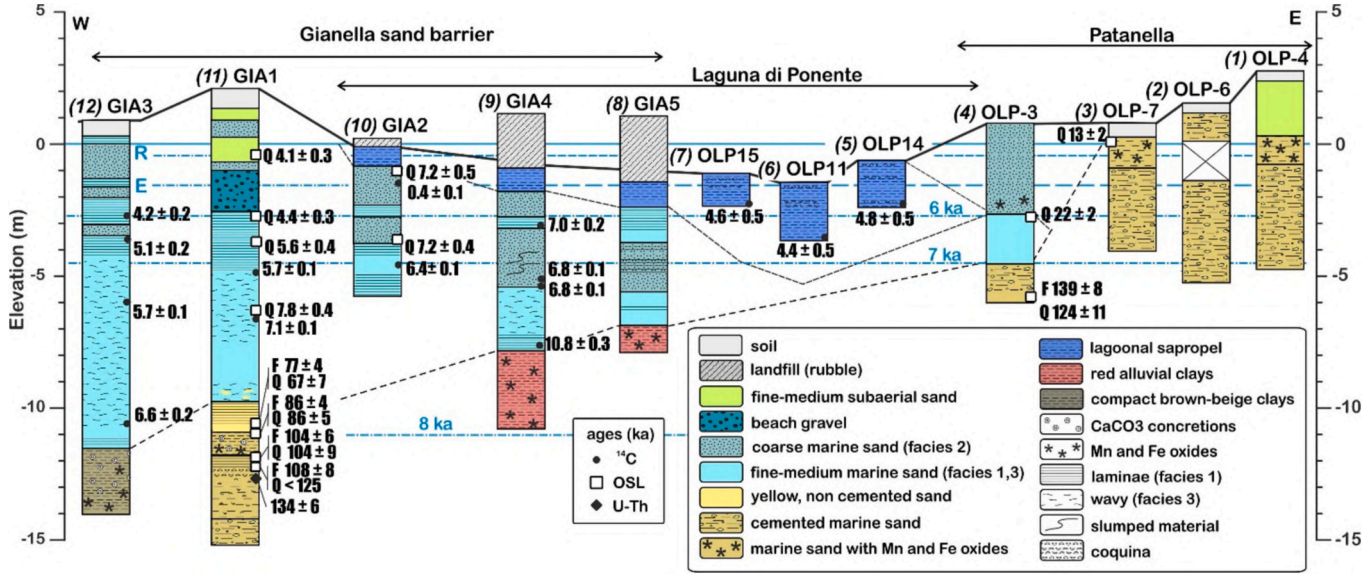

Fig. 4. Distribution of sediment facies and ages along a core transect from the Patanella bank to the Giannella sand barrier. Black long-dashed line: sequence boundary. Black, short-dashed line: base of lagoon layers. Blue dashed lines: sea level at successive 1 kyr time step according to the model of Roy and Peltier (2018). Roman (R) and Etruscan (E) levels from Leoni and Dai Pra (1997). (For interpretation of the references to colour in this figure legend, the reader is referred to the web version of this article.)

include a gravel bed in the Giannella SB (GIA-1, Fig. 4), and heavy mineral placers in the eastern part of the Feniglia SB.

The Feniglia and Giannella SBs both lie on a sandy substrate indurated by compaction and carbonate cementation/concretionning. This type of induration is commonly observed in marine sands deposited during earlier sea level highstands along the coast of Tuscany (Funiciello

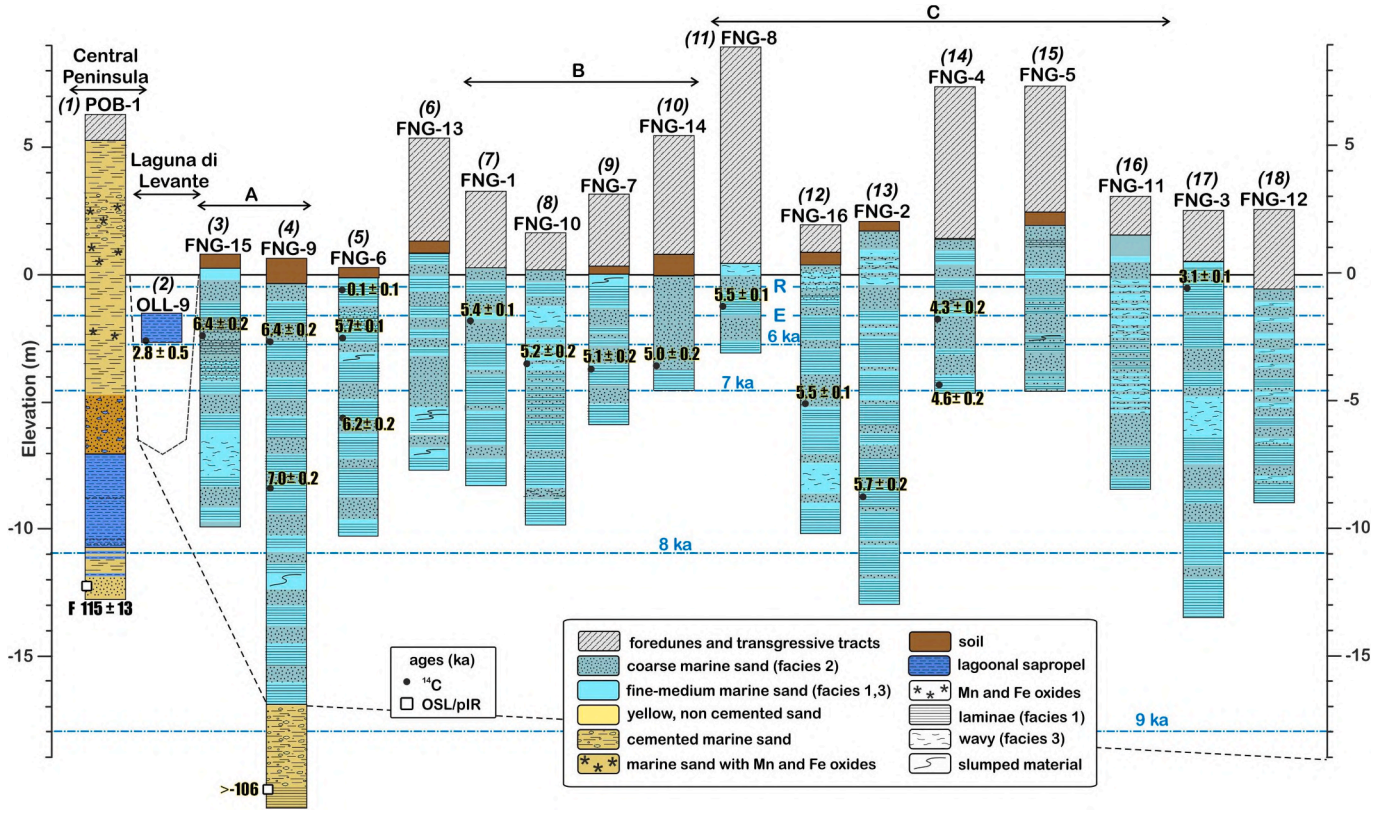

Fig. 5. Distribution of sediment facies and ages along a core transect from the Central Peninsula to the Feniglia sand barrier. Italic numbers in brackets next to core names: core locations of Figs. 4 and 5. Black dashed line: sequence boundary. A, B, and C: beach ridgelines (Fig. 2C). Black long-dashed line: sequence boundary. Black, short-dashed line: base of lagoon layers. Blue dashed lines: sea level at successive 1 ka time step according to the model curve of Roy and Peltier (2018). Roman (R) and Etruscan (E) levels from Leoni and Dai Pra (1997). (For interpretation of the references to colour in this figure legend, the reader is referred to the web version of this article.)

et al., 2020). They also crop out along the central peninsula of Orbetello, where they exhibit steeply-dipping (10–30°) planar cross-stratification (Coltorti and Ravani, 2017) typical of the *Sabbie di Doronatico* aeolian formation (Pasquetti et al., 2020). The sediments that we cored between the lagoon of Orbetello and the Albegna River (Fig. 2D, Patanella; Fig. 4) also consist of indurated sands. These latter, together with the sands encountered below the Holocene sand barriers, differ from those of the central peninsula in that they only exhibit horizontal planar stratification, and laminae similar to facies 1, suggesting that they were deposited instead in beach/shoreface environments (Fig. 3E).

Holocene silts and sandy clays are restricted to the lagoon of Orbetello, where they display alternations of shell-rich, organic sapropels and coquina beds (Fig. 3F). These lagoonal deposits do not extent onshore in any direction around the lagoon, except maybe in the north, where they could connect, via a narrow corridor, to the Albegna River floodplain and its underlying lagoonal clays (core ALB1 (Chapkanski et al., 2021)). Older, shell-rich lagoonal clays were only cored in one instance, between −7 and − 11 m below the central peninsula (core POB-1, Fig. 5). Massive fluvial red clays were reached below the Holocene Giannella SB in cores GIA4 and 5, at the toe of Monte Argentario (Fig. 4). These clays are derived from red soils (*terra rossa*) that mantle the Triassic limestones on Monte Argentario. They were deposited on alluvial fans over the emerged Last Interglacial (LIG) shelf during the last glaciation.

4.2. Dating

Holocene sand barrier ages provide minimum limiting indicators of past sea level. We therefore used regional curves of sea level rise as a first-pass screening test of age reliability (Fig. 6A). These curves, R and V (Roy and Peltier, 2018; Vacchi et al., 2016), were generated using the ICE-5G VM2 and ICE-7G_NA glacial isostatic models, fitted to northern Latium sea level indicators, 70 km to the south of Orbetello. They are similar to those fitted to sea level indicators around the tectonically-stable Sardinia (Roy and Peltier, 2018; Vacchi et al., 2016), indicating that our study area has been tectonically stable during the Holocene. Additional constraints are provided by lower-limiting indicators of past sea-level located closer to Orbetello. The islet of Argentarola, next to Monte Argentario (Fig. 1A3), hosts karstic conduits which flooding chronology has been established by radiocarbon dating of calcite tubes secreted by marine serpulids that lived on their speleothems (Antonioli et al., 2001). Additional constraints are provided by the flooding and infilling of the Albegna River valley (Fig. 1A3), 8 km to the north of Orbetello (Chapkanski et al., 2021; Mazzini et al., 1999), and by transgressive lagoonal clays and their overlaying sand barrier (D'Orefice et al., 2020), 14 km to the south of Orbetello. These local indicators all lie close to the Northern Latium curve (Fig. 6A), confirming that the modeled curve is a good proxy for sea-level rise at Orbetello. Radiocarbon and luminescence ages from the Giannella and Feniglia SBs are in agreement with these earlier indicators, lying below, or slightly above the curve (Fig. 6B). They nonetheless include three outliers: ^{14}C samples GIA6–52 and FNG2–183 yielded recent ages despite being located within the older, inner parts of the sand barriers. For their proximity to the ground surface, we interpret them as contamination by loose topsoil during coring. Conversely, radiocarbon sample GIA4–806 yielded a transgression age 3 ky older than the regional curve (Fig. 6B). Its age implies either that the curve strongly underestimates the transgression age, or, more likely, that the sample contains older organic matter reworked during the transgression, as it lies only a few centimeters above the transgression surface.

Overall, the radiocarbon ages display a fairly good general

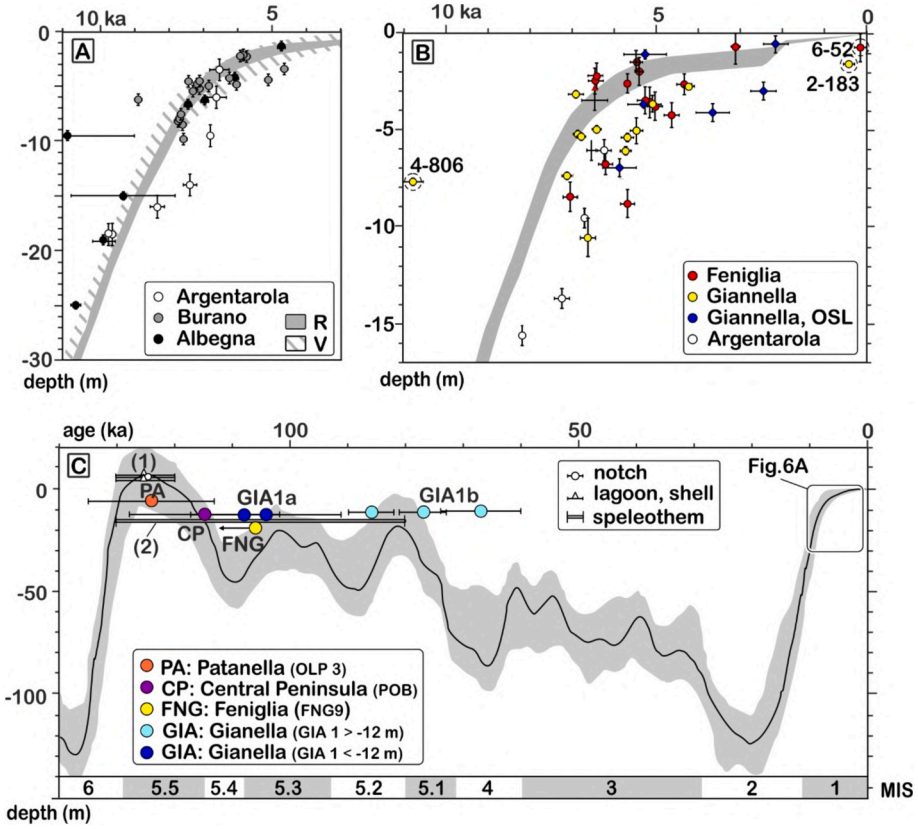

Fig. 6. Sea level rise curves compared to ^{14}C and OSL deposition ages in the sand barriers. A: Albegna estuary, Burano lagoon, and Argentarola cave post-glacial sea level indicators, plotted against the modeled sea level curves for the Northern Latium (R and V, see text for references). Sample numbers refer to outliers mentioned in the text. B: plot of Holocene ^{14}C (all symbols but blue) and luminescence ages (blue) ages of marine samples vs. depth, relative to the Roy and Peltier (2018) curve, modified over the past 2.5 kyrs to include local archeological constraints from Leoni and Dai Pra (1997). C: Sea level curve of the past 130 ky (Waelbroeck et al., 2002), and last interglacial local sea level indicators: notch and marine/lagoonal fauna (Nisi et al., 2003), interrupted speleothem growth, Argentarola cave (Antonioli et al., 2004), and OSL data (this study). MIS: marine isotopic stages. (For interpretation of the references to colour in this figure legend, the reader is referred to the web version of this article.)

stratigraphic consistency along single cores and from one core to the next (Figs. 4 and 5). They display progressive younging seawards, and an age distribution consistent with the location of each core with respect to the beach ridgelines visible on the LiDAR topography (Fig. 2B, C): in the Giannella SB, radiocarbon ages are synchronous along strike in the ridge that links core GIA1 to core GIA3, and in the ridge that links GIA2 to GIA 4 (Figs. 2B and 4). Likewise, in the Feniglia SB, ages at any specific depth are also synchronous within uncertainties along beach ridge A (Figs. 2C and 5). In ridges B and C, ages are only slightly diachronous beyond uncertainty (0.2 kyr), except in core FNG-4, where 1 kyr younger ages are found. Ages do not vary in any consistent nor significant manner along strike, discarding progressive down-drift barrier lengthening as a growth mechanism (Fig. 1B). Luminescence ages are consistent with radiocarbon ages (Fig. 4), except in core GIA-2, which yielded both exceedingly old luminescence ages and exceedingly young radiocarbon ages.

A large gap is observed between the OSL/pIR ages of the Holocene sand barriers and those of the underlying marine sediments, which span MIS 5 (130–75 ka, Fig. 6C). These MIS 5 ages are consistent with MIS 5 representing the last time sea level rose high enough to flood the saddle between Monte Argentario and the mainland (Fig. 6C). Argentarola cave flooding data confirm that sea level was above −20 m from 126 to 80 ka (Antonioli et al., 2004). The U/Th coral age of 134 ± 6 ka (−12.5 m) obtained below the Giannella SB is in agreement with overlying luminescence ages of >125 ka on quartz and 108 ± 8 ka on feldspar between −12.5 m and − 12.0 m (Fig. 6C, GIA1 < 12 m). These U—Th and luminescence ages were obtained in indurated sands that are overlain, above −12 m, by a peculiar unit composed of laminated, poorly cemented, yellowish sands that yielded OSL/pIR ages of 67 ± 7 to 86 ± 5 ka (Fig. 6C, GIA1 > 12 m). The latter could have been deposited during one of the relative highstands that punctuated sea level drawdown at the beginning of the last glaciation, when sea level rose repeatedly above –20 m (Wohlfarth, 2013), specifically during MIS 5.3 (108–102 ka) and MIS 5.1 (86–75 ka, Fig. 6C). Alternately, as this unit directly lies on the cemented sands, it could contain large amounts of reworked MIS 5 sand, only partially reset during the Holocene transgression. The compacted and cemented sands that underlie the Feniglia SB yielded an MIS 5 OSL age of >106 ka (close to saturation) at −20 m. They may have been deposited during MIS 5.5 or 5.3 (Fig. 6C). The central peninsula of Orbetello yielded at −12 m an pIR age of 115 ± 13 ka, consistent with the ascription by earlier authors of the overlying cemented sands to the last interglacial (MIS 5.5, Fig. 6C). Cemented sands in the cores located between the Albegna River and the lagoon of Orbetello yielded ages of 139 ± 8 ka (pIR) to 124 ± 11 ka (OSL) at −6 m, consistent with deposition during MIS 5.5 (Fig. 6C). Albeit extracted from marine sands, two OSL samples yielded ages inconsistent with deposition in a marine environment. These samples are located close to the ground surface in OLP-3 (3 m, 22 ± 2 ka) and OLP-7 (0.5 m, 13 ± 2 ka). The LiDAR topography shows traces of quarrying and landfilling in this area, which may have partially reset these ages.

4.3. Marine profiles

Acoustic profiles perpendicular to the sand barriers (Fig. 7A, B) show that the shoreface is underlain from– 3 to −15 m by oblique, shallow-dipping (Giannella: 0.6°, Feniglia: 0.8°), quasi-planar reflections, with

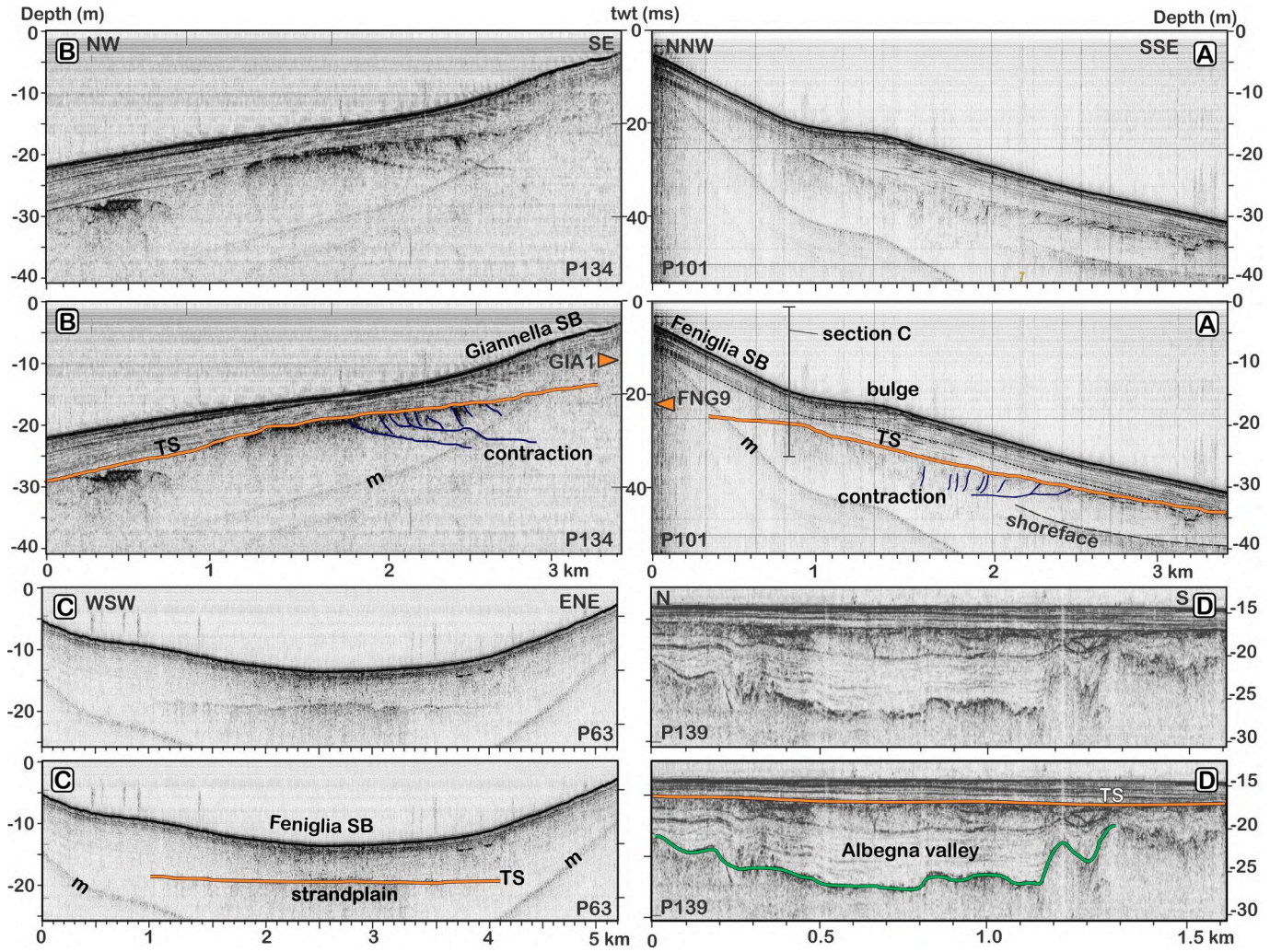

Fig. 7. Raw and interpreted 3.5 kHz offshore acoustic profiles across the Feniglia (A) and Giannella (B) sand barrier shorefaces (location: Fig. 2A). TS: transgression surface. m: first multiple. Orange triangle point to the depth of the depth of the transgression surface in cores onshore.

a 10–20 cm vertical separation. These reflections produce a tangential downlap pattern over an acoustic basement that rises landwards, reaching - 15 m in front of the Giannella SB and − 19 m in front of the Feniglia SB. The rising acoustic basement projects onshore to the depth at which MIS 5 cemented sands were encountered by coring at −11 m and – 17 m, respectively. The top of the acoustic basement is therefore interpreted as the Holocene transgressive surface, as in earlier seismic profiles acquired across the Feniglia shoreface (Tortora, 1989; Tortora, 1996a). It can be traced downslope to the sequence boundary SB1 on the marine shelf off the Giannella SB (Ridente et al., 2012), and to the sequence boundary W off the Feniglia SB (Chiocci, 2000; Fraccascia et al., 2013). The overlying oblique-tangential reflections as likely produced by the alternation of facies 2 and facies 1 or 3 within the sand barriers.

The Holocene shoreface deposits thin out seawards, becoming only 5 m thick 1.0 to 1.5 km offshore. The dip of the Holocene reflections then decreases markedly to 0.3° below −15 m, under a seafloor composed of sandy silt (30–70 % sand) (Borelli et al., 1986). Off the Giannella SB below −15 m, the Holocene set drapes a slightly convex transgressive surface which thickness slightly increases farther offshore. Off the Feniglia SB, the downlap pattern extends farther offshore than off the Giannella SB. It is associated to shallower-dipping beds than those of the Feniglia upper-middle shoreface. The Holocene set pinches out 3.7–4.1 km offshore, like on earlier Uniboom seismic profiles (Tortora, 1996b). Farther offshore over the shelf, only a patchy, irregular, <1 m thick condensed Holocene layer is present. The distal, shallow-dipping Holocene wedge of the Feniglia SB is separated from its steeper-dipping shoreface by an 8 m-thick sediment bulge between −15 and − 25 m.

Off the Feniglia SB, the post-glacial transgressive surface rises steadily up to -19 m, 1 km from the shore, before becoming subhorizontal closer to the shore. Onshore, cemented sands are encountered by coring at −17 m (core FNG-9) indicating that the transgression surface remains subhorizontal below the sand barrier. Profiles parallel to the shoreline (Fig. 7C) show that the surface is also horizontal alongshore, contrasting with the overlaying parabolic reflections produced by the seaward-concave sand barrier clinoforms. The horizontal surface is underlain by marine sands (core FNG-9) and therefore interpreted as a former strandplain. Farther offshore, below the transgression surface, a series of concave, imbricate, C to S-shaped reflections dip landwards at 3–7°; they crosscut a 6 m-thick granular seismic facies. We tentatively interpret this structure as imbricate thrusts, affecting an internally-deformed Pleistocene sedimentary sequence. The thrusts are rooted in a subhorizontal to shallowly landward-dipping basal décollement, an arrangement typically produced by shallow contraction. Similar structures are present below the transgression surface off the Giannella SB (Fig. 7B), and are likewise interpreted as shallow contraction.

A profile was also acquired across the Albegna River mouth, parallel to the coast (Fig. 7D). It shows a ancient valley of the Albegna River incised into the shelf. The valley possesses a basal strath lying at −27 m, overlain by 10 m of deposits below the Holocene transgression surface.

This valley is not as deep as the > − 45 m deep Albegna River valley cored 5 km upstream, which was flooded and filled during the Holocene transgression (Mazzini et al., 1999). The valley imaged here is therefore interpreted as an older valley, filled with sediments up to ≥ − 20 m before the pre-Holocene Albegna valley was incised.

4.4. Lagoonal profiles

The lagoonal profiles reached a penetration depth of 12 m below the lagoon floor, in water depths ≥1 m. No acoustic penetration was obtained at shallower depth. Large areas of the *Laguna di Levante* subbasin are underlain by gas-rich layers that prevented imaging under 1 to 4 m below the lagoon floor. In the easternmost part of the *Laguna di Levante* subbasin, a highly reflective, shell-rich reflector located directly on the floor of the lagoon also hindered acoustic penetration. In all other parts of the lagoon, acoustic profiles revealed the sedimentary architecture of the barriers, back-barriers and their substrate (Fig. 8E, F, G). The lagoon floor is underlain by continuous, subhorizontal reflections with a vertical separation as tight as 10 cm. Within the cores, these reflections correspond to alternations of carbon-rich and shell-rich silty clays. The lagoonal reflections exhibit an extensive toplap pattern that records progressive, kilometer-scale expansion of the lagoon over both the central peninsula and the Holocene sand barriers. The earliest lagoonal layers were deposited at– 6 m behind the Giannella SB (*Laguna di Ponente*), and possibly as deep as – 8 m under a gas-rich region behind the Feniglia SB (*Laguna di Levante*). Stacked, seaward-dipping reflections are imaged inside the Giannella SB within 2–3 m of its surface (Fig. 8E). Their 2–4° dip is similar to the slope of the modern Giannella beach. They are therefore interpreted as earlier beach clinoforms. Their overlying unconformity, which is onlapped by the lagoonal layers, is interpreted as the strandplain surface, flooded and then buried below the lagoonal clays.

While the Feniglia SB appears to have nucleated directly on the flank of the central peninsula, the Giannella SB was built in front of a series of elongate narrow ridges, parallel to it (Figs. 8E, F, 9). With an amplitude of 3–4 m and a wavelength of 50–100 m, these ridges stand out as more prominent than the beach ridges of the Holocene Giannella strandplain. They are rather similar to its foredunes (Fig. 2B). Their transparent seismic facies resembles that of the cemented sands of the central peninsula. For this reason, and because they lie in the continuation of a MIS 5 sand barrier located farther north (see discussion), we interpret these ridges as foredunes of an earlier sand barrier, buried under the lagoon. Cementation prevented their complete levelling during their short-lived exposure to sea waves at the time of the Holocene maximum flooding. Landward of these old dunes, the Holocene lagoon layers lap onto the flank of the central peninsula, over a surface (L) under which lies a seismically transparent, 1 m-thick layer that contains a few irregular, surface-parallel reflections. This layer truncates an earlier set

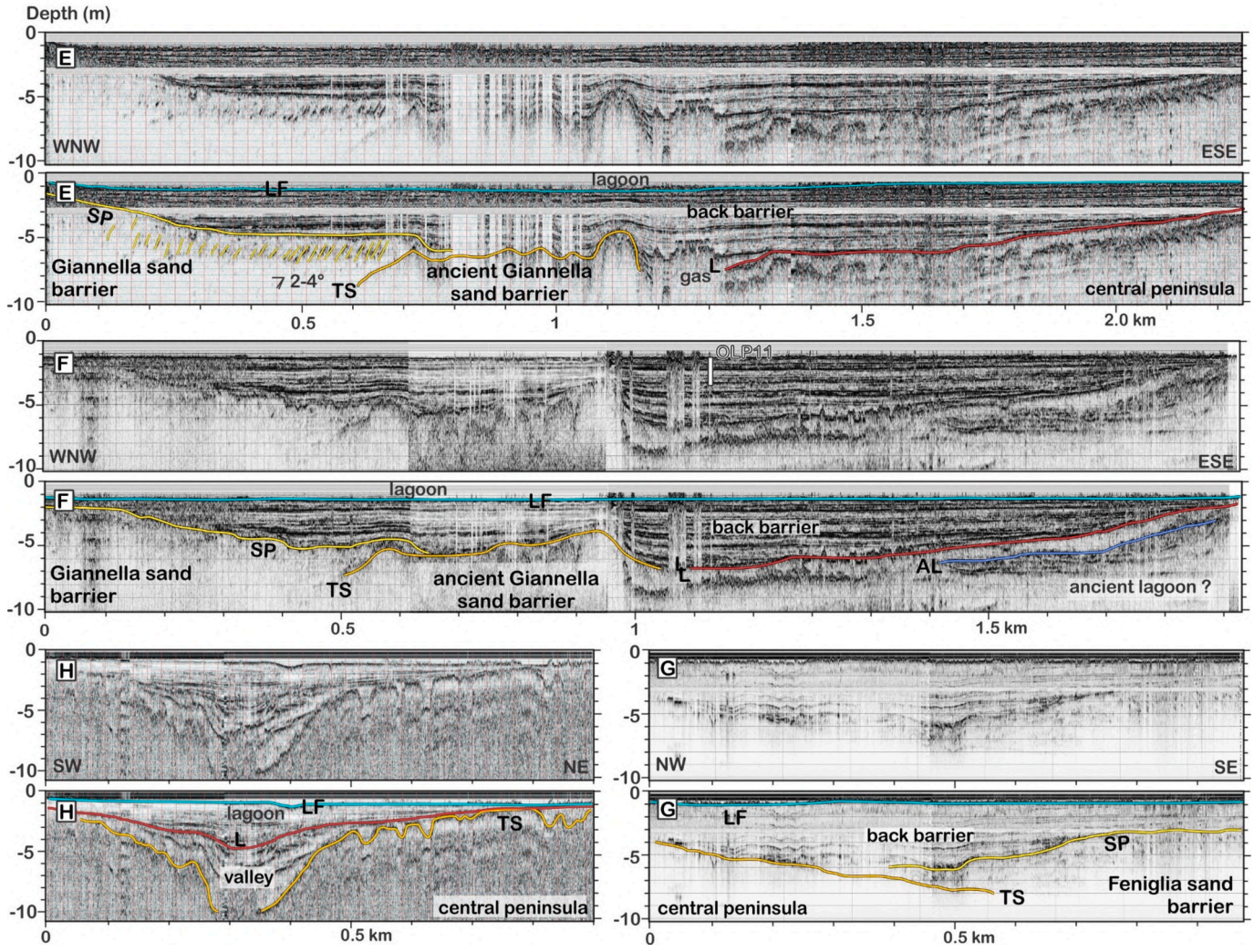

Fig. 8. Raw/interpreted 10 kHz acoustic profiles across the lagoon of Orbetello (location: Fig. 2A). Lines: AL: erosion surface of ancient lagoon layers, L: base of modern lagoon layers, LF: lagoon floor, SP: strandplain, TS: transgression surface.

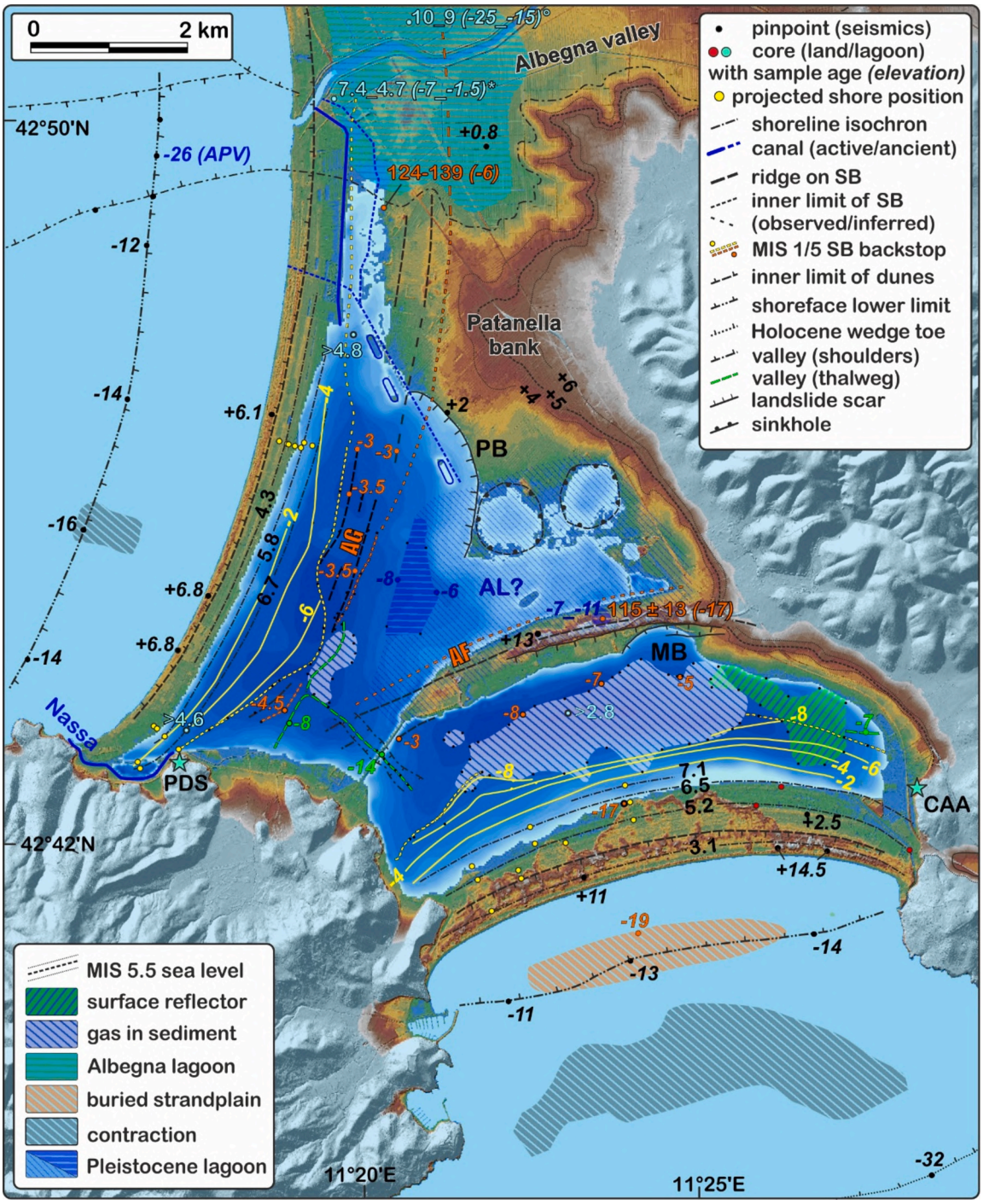

Fig. 9. Map of the tombolo of Orbetello showing morphological features emplaced since the last interglacial. Numbers in italic: elevations amsl in meters (black: modern surface; green: MIS 4–2 paleovalley thalwegs, yellow: contour lines on MIS 1 ridge plain surfaces; orange: MIS 5 surfaces; blue: ancient lagoon layers), other numbers: age in ka of samples dated in this study (with elevation in italic) and of calculated paleoshoreline positions. Earlier published ages from: ° (Mazzini et al., 1999), *: (Chapkanski et al., 2022). AG: ancient Giannella, AF: ancient Feniglia, AL?: putative ancient lagoon, APV: Albegna paleovalley; CAA: Cosa-Ansedonia aquifer; MB: La Madonnella Bight; PB: Patanella Bight; PDS: Punta degli Stretti cave. (For interpretation of the references to colour in this figure legend, the reader is referred to the web version of this article.)

of subhorizontal reflections, which seismic facies resembles that of the Holocene lagoon. These horizontal layers are therefore interpreted as an ancient lagoonal succession cut by a wave ravinement surface blanketed by a sand sheet.

The height of the central peninsula steadily and irregularly decreases along-strike, from the mainland to its tip, such that the peninsula can be expected to continue at shallow depth beneath the lagoon, all the way to Monte Argentario. The acoustic surveys (Fig. 8H) confirm that the peninsula is shallowly buried, but also show that it is incised by a deep valley which lowest part is filled by a transparent seismic facies with irregular reflections are interpreted as marine sand deposited below the first lagoonal layers at −6 m. The presence of this valley implies that the two subbasins of the lagoon have always been connected across the central peninsula ever since the lagoon has formed.

5. Discussion

To track the formation and development of the double tombolo, we combine together the sedimentary architecture revealed by acoustic imaging, core stratigraphy, and sediment age. We first discuss how the sand barriers formed and thickened (5.1), showing that they did not grow lengthwise and down-drift, as previously thought, but crosswise instead, forming large regressive strandplains on the flanks of the central peninsula. We then investigate how the lagoon developed between these strandplains (5.2), showing that it flooded the back barriers in a context of slowing sea level rise, making the strandplains look like offshore barriers. We then discuss the origin of the central peninsula (5.3), showing that it is a composite body, shaped through successive high-stands during MIS 5. We then review how this MIS 5 accumulation was reshaped during the last glaciation (5.4), before discussing to which extent inherited topography and the accommodation-supply balance each contribute to the formation of double tombolos (5.5).

5.1. Formation of the double tombolo by regressive sand barrier growth

Earlier studies advocated that the Giannella and Feniglia SBs began to form after the last glaciation. Initially, they would have formed sand spits that expanded from the mainland toward Monte Argentario over the millennia following the slowing down of the post-glacial transgression (Coltorti and Ravani, 2017; D'Orefice et al., 2022). Upon reaching Monte Argentario, the sand spits thickened seawards, becoming regressive sand barriers. Our data show that sand deposition ages do not vary along strike: among the oldest still-emerged beach ridges, ^{14}C ages only vary by 0.2–0.4 ky along strike. More substantial and systematic age gradients would be expected if the barriers had grown mostly by sand spit lengthening.

The earlier models that resorted to offshore sand barrier formation relied on previous observations on barrier evolution made farther south along the coast, where the remnants of overwashed transgressive barriers have been imaged at −25 m on seismic profiles (Tortora, 1989; Tortora, 1996a), and where coring and ^{14}C dating in modern barriers have shown that barriers initially transgressed their back barrier before growing upwards and then seawards (D'Orefice et al., 2020; Funiciello et al., 2020). In Orbetello, by contrast, no such initial stepping of the sand barriers over the lagoonal layers is observed: the acoustic profiles and the cores both show that no lagoonal clays are present under the sand barriers. Instead, the sand barriers are overlain by lagoonal muds from their land side all the way to the central peninsula, the lagoon layers overlapping the sand barriers over more than a kilometer (Fig. 10). Acoustic imaging further shows that the sand barriers contain seaward-dipping clinoforms that are typical of strandplain progradation (Berton et al., 2019; Billy et al., 2014; Oliver et al., 2017). They do not show patterns typically associated with landward or upward enlargement of sand barriers, such as landward-dipping clinoforms produced by overwash deposits (Barboza et al., 2021; Berton et al., 2019; Cooper et al., 2018; Garrison Jr et al., 2010; González-Villanueva et al., 2009; Rosa et al., 2017; Thom, 1984) expected in particular if the barriers had remained shallowly or periodically submersed. Studies of particle size distribution across the shelf, south of the Feniglia SB, have shown that sand in the Feniglia SB shoreface is currently provided by rivers feeding the southern littoral cell, which bypasses the Cape of Cosa-Ansedonia above −20 m. The relict transgressive sands that blanket the shelf do no currently feed the barrier (Tortora, 1989; Tortora, 1996b). The sediment bulge identified on the acoustic profiles at −15 to – 25 m (Fig. 7A) is composed dominantly of fine sand and lesser amounts of coarser sand (Tortora, 1996b). It lies below the depth at which the cape of Cosa-Ansedonia ceases to protrude above the seafloor, and at which it is wrapped by a faint moat at -20 m (Brocard and Conforti, 2023). The bulge therefore appears to be fed by deep longshore drift around the cape. From the bulge, the sediments are redistributed downslope to the distal wedge (Tortora, 1996b), and possibly partially upslope to the proximal wedge (Anthony and Aagaard, 2020; Kinsela et al., 2016), although most of the coarser shoreface sands bypass the cape of Cosa-Ansedonia at shallower depth (Tortora, 1989). The lack of discernible age gradient along the sand barriers can be explained by rapid accretion of each beach ridge under elevated sand influx, possibly combined, during early accretion, with more substantial contribution of wave-driven, onshore-directed sand upwelling.

Ridge plain elevation rose over time, accompanying sea level rise from – 7 ± 1 m to its current level. The accretion style did not change over the 1.8 km of Feniglia SB progradation and 1.1 km of Giannella SB progradation (Fig. 10): under the lagoon, beach profiles produce 2–4° seaward-dipping reflections. Across the still-emerged parts of the strandplains, beach stacking is manifested by ridges <2.5 m in height (Fig. 2B, C), which coring shows to be underlain by shallow dipping (<5°) planar sand beds. Offshore, below the current shoreface, progradation is evidenced by the downlap of 0.6–0.8° seaward-dipping reflections onto the transgression surface.

Regional sea level curves (Fig. 6A) and initial shoreline depths suggest that barrier accretion started 6–7 kyr ago, during a threefold reduction in the rate of sea level rise. It is a time of global ridge plain initiation (Roy et al., 1980; Thom, 1984), and the time of sand barrier stabilization south of Orbetello (D'Orefice et al., 2020). We assessed the rate of progradation of the Giannella and Feniglia strandplains using the distribution of their ^{14}C ages. Current sample depth, age, and contemporary sea level according to the curve of Roy and Peltier (2018) were used to estimate their depositional depth. Then, using present-day shoreface gradients, we reconstructed the distance of the samples to their contemporary shoreline (Table S2–1). These reconstructed distances were then used to draw paleo-shorelines on sections and maps (Figs. 9 and 10). Finally, these paleo-shoreline positions were used to quantify accretion rates between 7.1 ka and 3.1 ka.

The oldest emerged part of the Giannella SB next to the lagoon of Orbetello was emplaced 4.8–4.3 kyr ago, while its Feniglia SB counterpart was emplaced 7.1–6.5 kyr ago. The successive paleo-shoreline positions imply a decrease in progradation rate from 180 m/kyr between 6.8 and 5.8 ka down to 70 m/kyr over the past 4.3 kyr along the

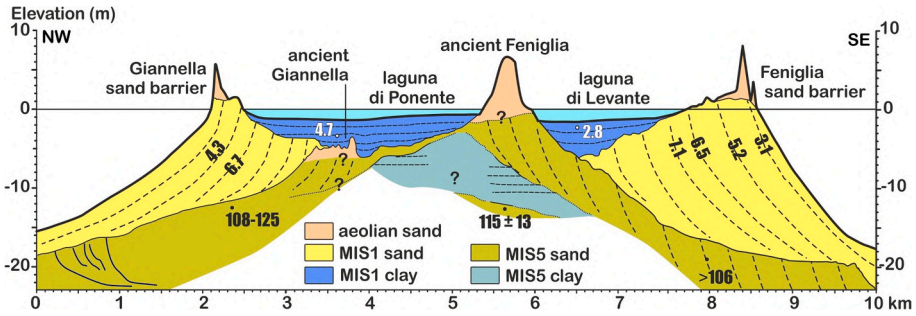

Fig. 10. Synthetic section across the peninsula of Orbetello, showing the main elements of its sedimentary architecture. Numbers in bold indicate accretion age (in ka) based on ^{14}C, luminescence, and U—Th ages.

Giannella SB. Along the Feniglia SB, progradation likewise slowed from 220 m/kyr between 6.5 and 5.2 ka down to 30 m/kyr over the past 3.1 kyr. If both strandplains initiated 6–7 kyr ago, as suggested by the sea-level curve (Roy and Peltier, 2018), then extremely fast rates of initial progradation are required for the strandplains to reach in time our oldest reconstructed shorelines. However the position of the oldest reconstructed shoreline is also the most sensitive to the choice of the transgression age provided by the curve (Roy and Peltier, 2018), and to the time elapsed between organic sample formation and sample deposition (considered to be negligible). An earlier transgression time, or/and the incorporation of a delay between ^{14}C sample formation and deposition both dampen the calculated deceleration in strandplain progradation, without fully suppressing it.

Prominent foredunes were emplaced over the Feniglia and Giannella strandplains during the past 3 kyrs (corresponding to 10–15 % of strandplain width accretion). Shifts from low-lying beach ridges to tall foredunes are commonly associated to slowing progradation (Carvalho et al., 2019; Ciarletta et al., 2019; Psuty, 2008) and may therefore be a consequence of the reduction in progradation rate. Alternately, the shift to taller foredunes may result from anthropogenic disturbance along the upper shoreface/foredune interface (Oliver et al., 2017). This latter possibility cannot be ruled out here as it could reflect increasing anthropogenic influence during the Early Bronze Age.

Rapid initial strandplain progradation followed by sharp deceleration is common (Dillenburg et al., 2020; Kinsela et al., 2016; Oliver et al., 2020; Roy et al., 1980; Stive and De Vriend, 1995; Thom, 1984). Under constant sand influx, progradation deceleration simply results from barrier progradation into deeper water. Nonetheless, initial rapid progradation has been frequently ascribed to the accretion of large volumes of sand previously stored over the shelf, transported landwards either by barrier overstepping/rollover during the transgression, or by cross-shore upwelling during the following highstand (Cooper et al., 2018; Kinsela et al., 2016; Oliver et al., 2020; Roy et al., 1980; Thom, 1984). The ensuing deceleration has been ascribed to the exhaustion of this sand reservoir, or to the attainment of beach profile equilibrium (Kinsela et al., 2016; Oliver et al., 2020; Roy et al., 1980; Thom, 1984). Off the Feniglia SB, relict shoreface sands cover the seafloor between −30 m and − 50 m (Tortora, 1996b). Their composition differs from that of the modern Feniglia SB, demonstrating that these relict sands do not currently feed the Feniglia SB. They form a thin blanket (Tortora, 1996b) indicating that this sand reservoir is currently exhausted -if it ever significantly contributed to the growth of the Feniglia SB. Decrease in accretion rate have also been ascribed to increasing sediment bypass around the headlands that bound sand barriers, as embayments become infilled (Kinsela et al., 2016). This does not apply to Monte Argentario, because water depths in excess of 50 m are maintained on its sea-facing side, and because the sands of the Feniglia SB are reportedly trapped behind the headland (Tortora, 1996b).

5.2. *The lagoon of Orbetello: landside flooding of the regressive barriers under rising sea level*

The earliest lagoonal layers were deposited more than −8 m below current sea-level. The extent of the overlap pattern over the central peninsula and the sand barriers implies that the lagoon started small, but expanded considerably. The regional sea level curves predict that the lagoon formed 7 ± 1 kyr ago (assuming tight coupling between sea-level and lagoon level). The cores provide a minimum initiation age of 2.8 ± 0.5 ka for the lagoon behind the Feniglia SB, based on a sample located at a depth that only represents 16 % of the total lagoonal sediment thickness. In the Giannella back-barrier, similarly, ages of 4.4 ± 0.5 ka and 4.8 ± 0.5 ka were obtained at 39 and 52 % of the lagoonal sediment thickness (Figs. 4, 5 and 9). The limited depth of the samples implies that lagoon initiation likely occurred much earlier. Besides, these ages are potentially underestimated, as no lagoonal carbon reservoir was added relative to the ocean ($\Delta R = 0$). During its expansion, a > 6.7 ka beach ridge on the Giannella SB (according to the reconstructed shoreline) was flooded into the lagoon before 4.6 ± 0.5 ka (^{14}C age of lagoon mud). The lagoon subsequently flooded the Bronze Age settlement of Santa Liberata after 2.9 ka (SL, Fig. 1A3), and finally a series of Roman farms on the Feniglia SB (Figs. 2C).

The flatness of the strandplains allowed the lagoon to spread considerably without gaining much depth. Sedimentation could have soon filled such a shallow lagoon, had slow deposition not allowed it to persist up to today: radiocarbon ages suggest sedimentation rates of 0.3–0.5 mm/y over the past 5 kyr that may be underestimated, no local carbon reservoir being added ($\Delta R = 0$). Such a slow sedimentation is expected nonetheless because the lagoon is flanked to the north and south by Holocene sand barriers, and to the west and east by small catchments, such that detrital influxes are limited. Unless assuming lagoon ^{14}C reservoir ages as large as 2–2.5 kyr –that is, larger than documented reservoir ages in Mediterranean lagoons (Sabatier et al., 2010)-, an overall decrease in sedimentation rate is documented within the lagoon. Under constant sediment flux, such a decrease may result from the increasing lagoon area. It may nonetheless reflect a decrease in sediment flux. In Orbetello, the only identifiable potentially dwindling contribution is that of the Albegna River. The river was thought to have built a large delta in the lagoon before being rerouted to its current course (Coltorti and Ravani, 2017; D'Orefice et al., 2022). However, cores OLP-3 to OLP-7 show that no delta ever existed there, the ground surface being directly underlain by cemented Pleistocene marine sands against which the Holocene Giannella SB is docked. Core ALB-1 shows that a 3 m-thick layer of <4.7 ka floodplain clays fills the saddle between the Holocene Giannella SB and the Pleistocene sands (Chapkanski et al., 2022). Through this narrow corridor, and in a context of otherwise low terrigenous input, the Albegna River may have contributed most clays and silts to the lagoon. The data at hand, however, do not reveal whether the Albegna fluxes decreased over time. Limited terrigenous fluxes allowed biogenic carbonate and organic matter production within the lagoon to become a non-negligible, albeit not dominant part of the lagoonal sedimentation (Bonanni et al., 1992). The lagoon is expected to deepen and widen as sea level continues to rise. Its deepening may be counterbalanced by accelerated sedimentation driven by farming, urbanization, and seawater/river water pumping.

5.3. *The central peninsula: a composite structure formed during MIS 5 highstands*

The central peninsula yielded a pIR age of 115 ± 13 ka, supporting the view that it is a Pleistocene sand body (Coltorti and Ravani, 2017; D'Orefice et al., 2022; Ferri and Pranzini, 2006; Mazzini et al., 1999). Rather than a central tombolo, however, it should more properly be regarded as the ancient Feniglia SB, its concave side similarly facing the southern littoral cell. Its prominent, irregular relief, and the common presence of cross-stratifications (Coltorti and Ravani, 2017) indicate that the emerged part of the peninsula is a flooded MIS 5 dune field, equivalent of the MIS 1 Feniglia foredune field. No MIS 5 Giannella SB seems to stand between the MIS 1 Giannella SB and the MIS 5 Feniglia SB. Instead, the MIS 1 Giannella SB is separated from the Feniglia MIS 5 SB by a smooth lowland area north of the lagoon (Patanella bank, Fig. 9 and 2: D). The surface of the latter lowers from +7 m in the east, down to +2 m next to the lagoon of Orbetello. Immediately behind the MIS 1 Giannella SB, the Patanella bank is riddled, over a width of 900 m, with low-lying, N-S-striking groves and ridges that rise from 0 next to the lagoon up to +4 m farther inland. These ridges lie in the continuation of a MIS 5.5 sand barrier located north of the Albegna valley (Mazzini et al., 1999; Nisi et al., 2003). The 139 ± 8 ka (pIR) and 124 ± 11 ka (OSL) ages obtained below these ridges (core OLP-3) support the view that the ridges represent the continuation of the MIS 5 barrier, south of the Albegna valley. Farther south, below the lagoon, the acoustic profiles reveal a series of ridges located immediately behind the MIS 1 Giannella SB (Figs. 8 to 10). We interpret these latter as the concave-to-

the west, MIS 5 Giannella SB, buried under the lagoon. The Giannella and Feniglia MIS 5 SBs both flank the Patanella bank. Coring shows that the MIS 5 Feniglia SB rests on lagoonal clays at −7 to −11 m (core POP-1) as well as on deeper 115 ± 13 ka sands. The clays may have settled in the back-barrier of the MIS 5 Feniglia SB. Horizontal reflections interpreted as lagoon layers occur behind the MIS 5 Giannella SB as well, although they are not directly overlapped by the MIS 5 Giannella SB (Fig. 8). Instead, they are crosscut by a ravinement surface (Zecchin et al., 2019) located farther inland. The MIS 5 Feniglia SB may lie on the same surface, above similarly eroded lagoonal clays. Sub-bottom imaging shows that the ravinement surface rises toward the Patanella bank, which smooth topography may therefore represent the emerged continuation of this marine surface. The Patanella bank was entirely flooded during MIS 5.5(Figs. 6C; 11A), when sea level reached 5 ± 1 m (Nisi et al., 2003), such that the ravinement surface may manifest the partial erosion of a pre-existing back-barrier synthem emplaced either early during MIS 5, or during a previous interglacial. The first earlier interglacial is unlikely, because during MIS 7 sea level remained below −15 m in the Argentarola Island cave (Antonioli et al., 2021). If the dunes of the ancestral Feniglia SB had been present at the time, they would have been largely submersed. It seems more likely, therefore, that a first phase of sea level fall allowed the ancestral Feniglia and Giannella SBs to form on the flanks of the Patanella bank (Figs. 6C and 11B). The corresponding sea level cannot be constrained precisely because the base of these dunefields is not visible. An extensive strandplain later formed at −19 m under the MIS 1 Feniglia SB (Figs. 7, 9 and 10). Its elevation corresponds to sea level during the highstand of substage MIS 5.3, in agreement with its luminescence age of >106 ka in core FNG-9 (Fig. 6C).

To sum up, our luminescence ages are in agreement with earlier models which stated that the central isthmus formed during MIS 5. Nonetheless, the LiDAR and acoustic data show that the central peninsula is not a simple tombolo, but rather a composite body, which complexity reflects the 50 kyr-long succession of relative sea level highstands and lowstands that precedes the main draw-down of the last glaciation.

5.4. *Reshaping of the central peninsula during the last glaciation and Holocene flooding*

The isthmus that had formed during MIS 5 was exposed to subaerial weathering and reworking during MIS 4–2. The flatness and permeability of its marine sands inhibited surface runoff and erosion, such that it retains much of its original marine morphological traits. Some streams draining Monte Argentario built clayey alluvial fans along its northern base (Fig. 4: cores GIA-4 and 5). Farther east, some of these streams joined to form an east-flowing river which incised a valley across the central peninsula (Figs. 8H and 10). Two shallow circular depressions 800 m across and 2 m deep formed north of the central peninsula (*Stagnone* and *Stagnino*, Fig. 9). They may represent sinkholes resulting from dissolution in Triassic limestones below the thick Pleistocene sedimentary cover. They may have hosted temporary playa-type lakes that enlarged the initial depressions. The isthmus was affected by gravitational spreading, possibly driven by the settling of MIS 5 layers

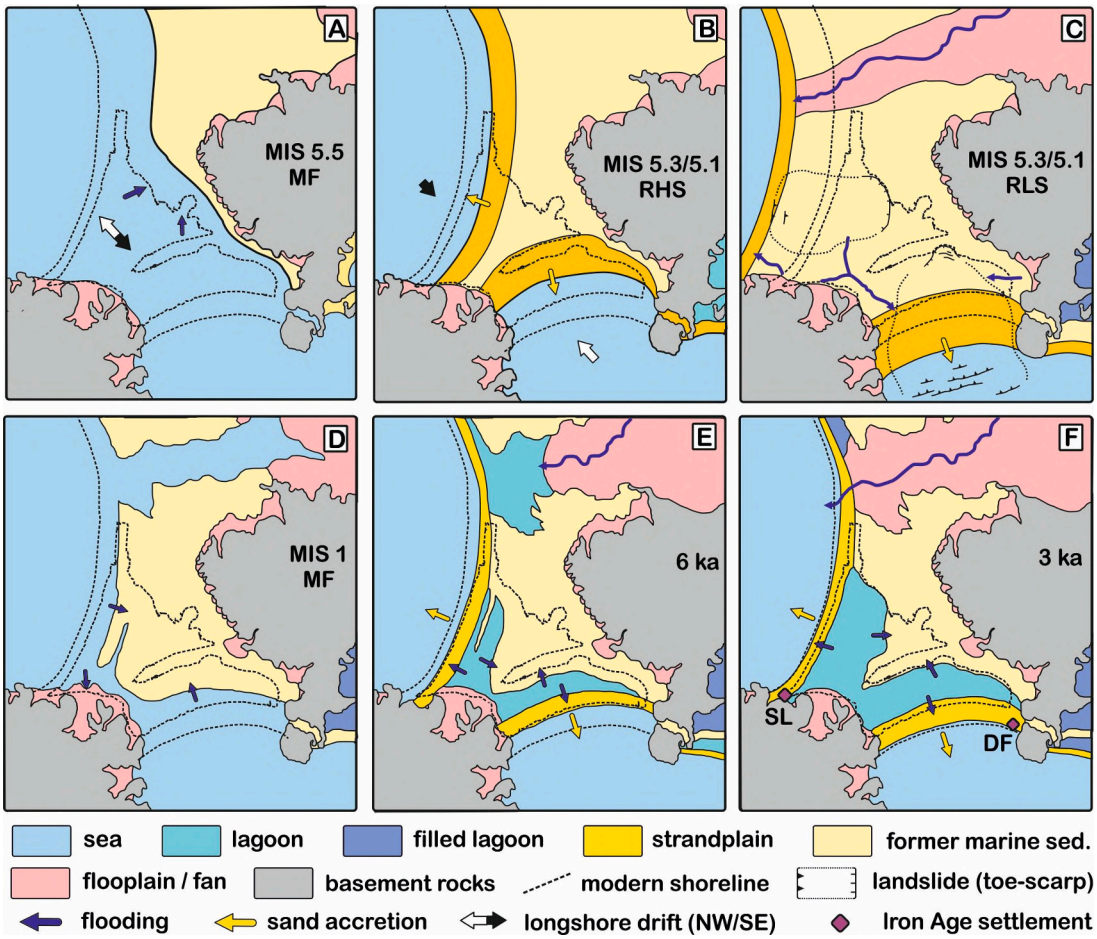

Fig. 11. Geographic evolution of the double-tombolo system of Orbetello. A: Last interglacial maximum flooding (MF, MIS5.5, ca. 130–120 ka); B: relative highstand (RHS) during MIS 5.3 to 5.1 stadial substages (ca. 100–80 ka); C: relative lowstand during MIS 5.3 to 5.1; D: Holocene (MIS 1) maximum flooding (MF); E: lagoon formation and expansion (6 ka); F: Late Bronze age (3 ka).

under their own weight after emergence, assisted by groundwater overpressure. The southern flank of the isthmus was scarred by an 800 m-wide bight (La Madonnella Bight, Fig. 9). The acoustic profiles imaged trenches as deep as 8 m opened into the pre-Holocene acoustic basement within the bight, which we tentatively interpret as tension cracks.

The concave-up, landward-dipping reflections that affect the pre-Holocene basement offshore may represent the corresponding contractional belt (Figs. 7 and 9) at the toe of the gravitational structure. Spreading only affected the least confined and least consolidated marine sediments, possibly over a décollement level rooted in lagoonal clays at −32 m. A similar contractional belt was imaged off the Giannella SB (Fig. 7B). The corresponding extensional area onshore would correspond to the 2 m-tall scarp that forms an arcuate 2 km-wide bight into the Patanella sand bank (Fig. 9). This bight has been previously interpreted as the concave flank of a cuspate Holocene delta, built by the Albegna River (D'Orefice et al., 2022). The scarp is not an erosional sea cliff, as its curvature does not conform to the curvature of the Giannella SB, nor an erosional lagoonal cliff, as lagoon waves are not even able to rework more recent non-cemented sands. If the interpretation of this scarp as a landside scar is correct, then the difference in elevation between the MIS 5 Giannella SB, buried below the lagoon at −3.5 m, and the MIS 5 Feniglia SB, which rises to +12 m above the lagoon, may be viewed as resulting, to some extent, from the settling of the MIS 5 Giannella SB relative to the MIS 5 Feniglia SB. The difference in height between the MIS 5 ridges in the north, near cores OLP 3–7, and the flooded MIS 5 Giannella SB in the south, suggests ~5 m of gravitational settling relative to the central peninsula. After the last glaciation, settling allowed partial flooding of the regressive sand barriers emplaced toward the end of the last interglacial. The sea flooded the valley incised during MIS 4–2 across the central peninsula, briefly isolating Monte Argentario from the mainland before the Giannella and Feniglia SB started to accrete (Fig. 11D). In the Late Bronze Age, their accretion had considerably slowed down, such that, by then, the landscape was not very different from today's (Fig. 11F).

5.5. *Double tombolo formation: supply-accommodation balance and inherited topography*

Starting from the case of Orbetello we discuss here how double tombolos form. We consider first the case of a single tombolo enlarging to form a double tombolo under continuously rising sea level. We show that such an evolution can simply accrue with alterations of the local sediment supply-accommodation balance, imparted by the development of the tombolo. We then elaborate on this model by adding the effects of sea level variations, looking at contribution of previously accreted tombolo morphology to later double tombolo formation under a variety of sediment supply conditions. We finally consider the duration of the double tombolo stage, as a function of the infilling rate of the back-barrier environment.

Tombolos are generated by the diffraction and refraction of waves around coastal islands, which promote the formation, in the lee of the islands, of submarine sand banks and emerged refraction salients that may evolve over time into fully emerged tombolos. The contribution of wave diffraction to these sediment accumulations prevails during the early stages, when seafloor remains deep between the islands and the mainland. Wave refraction contributes increasingly as banks shoal up (Flinn, 1997). The growth of the sand banks does not initially hinders net longshore drift between the islands and the mainland (Fig. 11A) (Franz et al., 2017). As shoaling progresses, however, the banks increasingly obstruct incoming waves in any direction, such that longshore drift away from the banks is suppressed, increasing net sediment fluxes toward the developing tombolos. Suppression is such that at some point it entrains net drift reversal toward the tombolos, down-drift of the dominant longshore flux (Franz et al., 2017). In the case of Orbetello, waves track dominantly from the south and west, generating northward-directed net longshore drift (Fig. 11A). Infilling of the strait during MIS 5 sheltered the NW side of the forming tombolo from south-tracking waves, allowing west-tracking waves to drive net south-oriented drift along the NW side of the tombolo. This reversal became effective at the latest once the tombolo had established a continuous land bridge between Monte Argentario and the mainland (Fig. 11B). The depth of the seafloor (−50 m) off Monte Argentario precludes longshore sediments bypass around this headland during sea level highstands. Even when sea level rises above −50 m, the promontory remains a zone of drift divergence to all dominant incoming waves. The contrasted mineral composition of the sands tracking from the south cell and from the north cell is reflected by the difference in the average total dose rate of the luminescence samples (Table S4–1), with is lower in the MIS 1 and MIS 5 Giannella sand barriers (1.3 ± 0.3 and 1.8 ± 0.4 Gy ka^{-1}), than in the MIS 1 and MIS 5 Feniglia sand barriers (2.8 ± 0.3 and 4.5 ± 0.7 Gy ka^{-1}).

Upon land bridge completion, tombolo flanks become terminal sinks for sediments brought in by the converging littoral cells. Under steady sea-level rise and net longshore flux, the ensuing retention of sediments promotes accelerated accretion and the development of regressive barriers rather than transgressive or stationary barriers (Ciarletta et al., 2020). It accounts for the early, rapid development of regressive conditions in the MIS 1 barriers of Orbetello, as opposed to the sand barriers located farther updrift, which tend to display more progressive shifts from transgressive to regressive patterns, followed by slower and more limited progradation (D'Orefice et al., 2020; Funiciello et al., 2020).

The formation of double tombolos is therefore naturally promoted, under rising sea level, by single tombolo completion, followed by rapid beach ridge stacking on both flanks (Fig. 12A). The resulting strandplains rise outwards, their surface elevation tracking sea level rise. Meanwhile the oldest and lowest parts of the strandplains become flooded, giving way to the double tombolo configuration. Tombolo enlargement is likely to be asymmetrical, reflecting differences in sediment fluxes between littoral cells. In Orbetello, the largest flux tracks from the south, and the asymmetry has led to 6 km of progradation across the Feniglia strandplain, as opposed to 1.5 km of progradation across the Giannella strandplain.

Double tombolo formation can occur according to this model entirely within the short duration of a single sea level highstand, provided that the tombolo is small, or that incoming sand fluxes are large enough. In most instances nonetheless, it is likely that highstand tombolos grow over several successive highstands, the Holocene tombolos thus growing over preexisting Pleistocene sandbanks or tombolos. Shallow previous highstand synthems affect Holocene highstand beach equilibrium profiles, promoting the anchoring of Holocene sand barriers onto Pleistocene basement highs (Brenner et al., 2015; Cattaneo and Steel, 2003; Cooper et al., 2012; Cooper et al., 2018; Otvos, 2020; Shawler et al., 2021). Barriers may then form some distance apart, also creating double tombolos (Fig. 12B). Along the coast of Tuscany, where the MIS 5 highstand stands 5 ± 1 m above current sea level, MIS 1 sand barriers lie seawards and downslope of MIS 5 barriers. Their location off the transgressive shoreline was controlled by the slope of the shelf, and by the translation of the shoreface equilibrium profile across the shelf during rising sea level (Brenner et al., 2015; Bruun, 1962; Cattaneo and Steel, 2003; Rosati et al., 2013). Up-drift of the Cosa-Ansedonia cape (Fig. 1A3), the MIS 1 sand barrier thus settled at a distance of ~300 m from the shoreline when barrier behavior reverted from retrogradation to progradation (D'Orefice et al., 2020). Likewise, a distance of 300 m to <500 m (under gas-rich profiles) appears to have initially separated the nascent MIS 1 Feniglia SB from the MIS 5 Feniglia SB. Conversely, because the vertical separation between the MIS 5 and MIS 1 Giannella SBs is opposite (the MIS 5 sand barrier culminating at −3 m, Fig. 9), the MIS 1 Giannella sand barrier grew anchored to the MIS 5 sand barrier. At places where sediment fluxes are more limited than at Orbetello, similarly anchored sand barriers may have formed over shallow Pleistocene highs, subsequently undergoing little progradation, if not retrogradation (Fig. 12B). This appears to be the case at Giens in France, which double

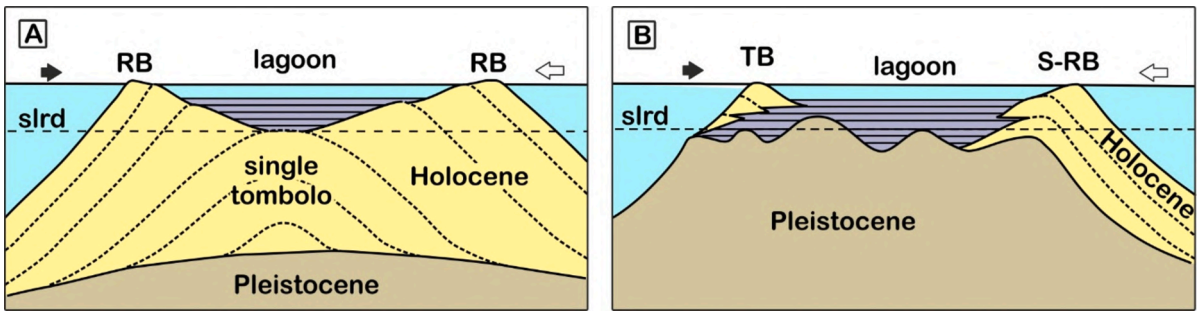

Fig. 12. Conceptual model showing the formation of a double tombolo composed of flooded regressive barriers (A), and transgressive, stationary to regressive barriers (B). slrd: sea level rise deceleration. RB: regressive barrier, TB: transgressive barrier, S-RB: stationary to regressive barrier. White/black arrows: dominant/minor longshore sediment flux.

tombolo combines a moderately regressive barrier up-drift to a transgressive barrier down-drift (Vella et al., 2000).

The conditions conducive to double tombolo formation reviewed here are frequently met. It should seem likely, therefore, that double tombolo formation is common, and could occur repeatedly during the enlargement of tombolos. The apparent scarcity of double tombolos, in this context, may be accounted for by the brevity of double tombolo stages, or/and by the geographically restrictive acceptation of the term (as two emerged sand barriers separated by an essentially unobstructed intervening body of water). The persistence of this restrictive configuration highly depends on the longevity of the body of water that occupies the back barrier. The latter is usually a shallow lagoon, prone to infilling. However double tombolo lagoons tend to receive less detrital sediments than their mainland counterparts because they occupy promontories flanked on two sides by sand barriers, and on a third side by a former island, of usually limited extent. Terrigenous sediments therefore mostly come from a short mainland stretch, which may either lengthen (e.g. former headland) or shorten (e.g. estuary) lagoon duration. As tombolos enlarge, central lagoons may form repeatedly each time new barriers are accreted. Such central lagoons, however, are likely to host an increasing number of obstructions as enlargement proceeds. If only earlier sand barriers emerge from the lagoons (such as is the case of Orbetello), the overall assemblage may well be described as a composite tombolo. On the other hand, if the central lagoon is cluttered with back-barrier landforms, the overall assemblage will no longer be regarded as a tombolo, but rather as a cape, or headland, surrounded by unrelated barrier-back barrier systems.

6. Conclusions

The double tombolo of Orbetello has been previously described as a transgressive to highstand Holocene sand accumulation, in which two sand barriers grew upward, some distance off an older central tombolo. The sand barriers would have grown from the mainland to the island of Monte Argentario, progressively enclosing a lagoon.

Using acoustic profiles, core stratigraphy and dating (^{14}C, OSL/pIR, U/Th), we show that the tombolos are large regressive strandplains, which initiated on the flank of the central tombolo and prograded seaward over large distances. They initiated early enough during the transgression for the oldest part to lie now at depths of - 7 ± 1 m. The lagoon in between them formed by drowning of the lowest, earlier parts of the strandplains.

The lagoon did not form by progressive enclosure, becoming increasingly isolated from the sea over time. Instead, it formed isolated and shallow, and has evolved by progressive enlargement and slow sedimentation, owing to very limited sediment supply. The lagoon persisted owing to sluggish rates of sedimentation over most of its existence, under slowly rising sea level. Its future evolution will be controlled by the balance between accelerating sea level rise, and potentially increasing detrital fluxes and biogenic production.

The acoustic profiles and sediment dating further show that the central peninsula of the lagoon is not a former tombolo, but a sand barrier emplaced on its southern flank during sea level fall, toward the end of MIS 5, on the flank of a much broader marine bank emplaced during the peak of the last interglacial (MIS 5.5: Eemian-Tyhrrenian). Its northern counterpart was found buried under the lagoonal sediments. The interruption of longshore sediment drift, across the central sand bank, created two terminal sinks on its flanks, taking the form of sand barriers. Their difference in size reflects the difference in size of the littoral cells that feed them. The faster accretion of sand on the south leads to a faster infilling of the space between the former island of Monte Argentario and the mainland there, as well as a strong asymmetry in tombolo development over time.

Owing to its location, composition, and subdued topography, the last interglacial synthem was little affected by stream incision and deposition, retaining most of its original landforms. It was also affected by a variety of other processes, such as deep karstification, wind deflation, and most notably, widespread, shallow landsliding. Upon the return of the sea in Holocene time, the sand barriers that flank the central sand accumulation resumed their growth in close proximity to the central peninsula. Monte Argentario very briefly became an island again, on account of the flooding of a valley incised in the central sand accumulation.

The double tombolo of Orbetello formed by widening of large strandplains under rising sea level, with lagoon formation by flooding of the oldest strandplain tracts. Their rapid development was assisted by the presence of the Pleistocene central tombolo, which obstructed longshore sediment drift, promoting rapid sediment accumulation on its flanks. In some cases, the presence of such a core may promote the formation of a lagoon behind highstand or transgressive barrier islands, anchored to a preexisting Pleistocene core. Lagoon formed behind regressive sand barriers are shallow and prone to quick shoaling by siltation, making such double tombolos short-lived stages in the process of tombolo growth.

Aknowledgments

We thank three anonymous reviewers for their insightful comments. This work was supported by the French ANR (Agence National de la Recherche), grant IDEX-Lyon Thalassocracies Sans Port, by the Université De Lyon (UDL), grant LabEx IMU (Intelligence des Mondes Urbains) Urbi et Orb(etello), by the French Oceanographic Fleet, campaign HISOPE (https://doi.org/10.17600/18002090), and by the Florida State University, grant Council on Research and Creativity (Cosa-Orbetello Lagoon). We thank Fabio Cianchi, Adriano Argenio, and the employees of the World Wildlife Fund (WWF) –Oasi di Orbetello, for logistical support. We thank Francesco Bottini and Enzo Danesi, from the Orbetello sailing club (Società Canottieri Orbetello), for their technical assistance during the coring in the lagoon and the Fishermen's Cooperative of Orbetello (Cooperativa Pescatori di Orbetello): Pier Luigi Piro

and Massimiliano Porti for their technical assistance during the lagoonal acoustic surveys. We extend our gratitude to Paolo Brama, Vittorio & Anna Fidati from the Orbetello Rotary Club, as well as Lamberto San Felice and his family, for facilitating and granting us access to private land for coring. We thank the laboratory REM/GEOOCEAN/ANTIPOD at the IFREMER, Brest, France, for the development, maintenance, and assistance in using the software QC_Subop for processing the 3.5 kHz acoustic data. Frederic Pinhal, Camille Gonçalves, Amber Goyon, and Matteo Pili for logistical help. We thank Daniele D'Ottavio (Geoambiente - Unigeo) for the excellent scientific coring.

We are grateful to the Nucleo Tutela Biodiversità Duna Feniglia (M. llo Vittorio Di Cori and his team) and the Department Biodiversità di Follonica (Col. t. Quilghini) for granting access the Duna Feniglia Protected area, the municipality of Orbetello (Andrea Casamenti and Ciara Piccini) and the harbor master's office and coastguards for providing access to the lagoon. We thank the soprintendenza Archeologia Belle Arti e Paesaggio per le province di Siena, Grosseto e Arezzo (Enrico Giuffre, Matteo Milletti, Salvadore Russo), the Istituto Centrale per l'Archeologia (ICA), the Soprintendenza per i Beni culturali e ambientali del Mare (Barbara Davidde) and Paolo Stefanini of the Tuscany region for facilitating access to protected areas onshore and offshore. Finally, we thank Claudio Calastri, Rita Deiana, Andrea Sposato, and Franco Buccianti for enriching discussions during this project.

CRediT authorship contribution statement

Gilles Brocard: Writing – original draft, Visualization, Supervision, Investigation, Funding acquisition, Formal analysis, Data curation, Conceptualization. **Jean-Philippe Goiran:** Supervision, Project administration, Investigation, Funding acquisition, Conceptualization. **Alessandro Conforti:** Writing – review & editing, Investigation, Data curation. **Frank Preusser:** Writing – review & editing, Formal analysis. **Quentin Vitale:** Writing – review & editing, Investigation, Formal analysis. **Guillaume Jouve:** Writing – review & editing, Software, Investigation. **Lionel Darras:** Investigation. **Christophe Benech:** Investigation, Funding acquisition. **Cécile Vittori:** Investigation. **Christine Oberlin:** Writing – original draft, Formal analysis. **Edwige Pons-Branchu:** Writing – original draft, Formal analysis. **Laurent Mattio:** Software. **Arthur de Grauuw:** Resources, Data curation. **Marco Leporati-Persiano:** Investigation. **Andrea U. De Giorgi:** Writing – review & editing, Project administration, Funding acquisition. **Adele Bertini:** Writing – review & editing, Supervision, Investigation.

Declaration of competing interest

The authors declare no competing interests.

Data availability

Supporting data are provided in the Supplementary Material document. SEG-Y and jpeg images of the sub-bottom profiles can be downloaded at https://doi.org/10.1594/PANGAEA.971980 (lagoon 10 kHz) and https://doi.org/10.1594/PANGAEA.971322 (offshore 3.5 kHz).

Appendix A. Supplementary data

Supplementary data to this article can be found online at https://doi.org/10.1016/j.margeo.2024.107415.

References

Anthony, E.J., Aagaard, T., 2020. The lower shoreface: morphodynamics and sediment connectivity with the upper shoreface and beach. Earth Sci. Rev. 210, 103334.
Antonioli, F., Silenzi, S., Frisia, S., 2001. Tyrrhenian Holocene palaeoclimate trends from spelean serpulids. Quat. Sci. Rev. 20, 1661–1670.
Antonioli, F., Bard, E., Potter, E.-K., Silenzi, S., Improta, S., 2004. 215-ka history of sea-level oscillations from marine and continental layers in Argentarola cave speleothems (Italy). Glob. Planet. Chang. 43, 57–78.
Antonioli, F., Furlani, S., Montagna, P., Stocchi, P., 2021. The use of submerged speleothems for sea level studies in the mediterranean sea: a new perspective using glacial isostatic adjustment (GIA). Geosciences 11, 77.
Barboza, E.G., Dillenburg, S.R., do Nascimento Ritter, M., Angulo, R.J., da Silva, A.B., da Camara Rosa, M.L.C., Caron, F., de Souza, M.C., 2021. Holocene sea-level changes in southern Brazil based on high-resolution radar stratigraphy. Geosciences 11, 326.
Bartolini, C., Corda, L., D'Alessandro, L., La Monica, G., Regini, E., 1977. Studi di geomorfologia costiera. III: il tombolo di feniglia. Boll. Soc. Geol. Ital. 96, 117–157.
Bellotti, P., Caputo, C., Davoli, L., Evangelista, S., Garzanti, E., Pugliese, F., Valeri, P., 2004. Morpho-sedimentary characteristics and Holocene evolution of the emergent part of the Ombrone River delta (southern Tuscany). Geomorphology 61, 71–90.
Berton, F., Guedes, C., Vesely, F., Souza, M., Angulo, R., Rosa, M., Barboza, E., 2019. Quaternary coastal plains as reservoir analogs: wave-dominated sand-body heterogeneity from outcrop and ground-penetrating radar, Central Santos Basin, Southeast Brazil. Sediment. Geol. 379, 97–113.
Bianchi, S., Biserni, G., Fanciulletti, F., Focardi, S., Marchetti, M., Nocchi, M., Pizzetti, E., Protano, G., Salleolini, M., Sandrelli, F., 2006. Studio idrogeologico finalizzato alla simulazione degli effetti dell'emungimento delle acque sotterranee da parte degli allevamenti ittici dell'area orbetellana e di Ansedonia, La Laguna di Orbetello: studi, ricerche, criteri e modalità di intervento in quattro anni di gestione commissariale 2003-2006. ColorDeSoli 167–176.
Billy, J., Robin, N., Hein, C.J., Certain, R., FitzGerald, D.M., 2014. Internal architecture of mixed sand-and-gravel beach ridges: Miquelon-Langlade barrier, NW Atlantic. Mar. Geol. 357, 53–71.
Blanc, J.-J., 1982. La dynamique littorale et ses applications sédimentologiques du grand Rhône à la presqu'île de Giens. Méditerranée 46, 25–33.
Bonanni, P., Caprioli, R., Ghiara, E., Mignuzzi, C., Orlandi, C., Paganin, G., Monti, A., 1992. Sediment and interstitial water chemistry of the Orbeteflo lagoon (Grosseto, Italy); nutrient diffusion across the water-sediment interface. Hydrobiologia 235, 553–568.
Borelli, G., Tortora, P., Burragato, F., 1986. Caratteristiche morfologiche, stratigrafiche e sedimentologiche della piattaforma continentale interna tra M. te Argentario e Torre Sant'Agostino. Mem. Soc. Geol. Ital. 35, 791–795.
Brenner, O.T., Moore, L.J., Murray, A.B., 2015. The complex influences of back-barrier deposition, substrate slope and underlying stratigraphy in barrier island response to sea-level rise: insights from the Virginia barrier islands, Mid-Atlantic Bight, USA. Geomorphology 246, 334–350.
Brocard, G., Conforti, A., 2023. Swath Bathymetry of the Gulf of Porto Ercole, Tuscany, Italy. SEANOE.
Bruun, P., 1962. Sea-level rise as a cause of shore erosion. J. Waterw. Harb. Div. 88, 117–130.
Campioltrini, G., 2019. Archeologia urbana ad Orbetello. In: Cardosa, M. (Ed.), Le antiche mura" etrusche" di Orbetello: atti della Tavola Rotonda. C&P Adver Effigi, pp. 93–111.
Cappietti, L., d'Eliso, C., Venturini, A., Valtriani, A., Tecch, M.-G., Aminti, P.L., 2006. Il model idraulico. In: Ludovico, A. (Ed.), La Laguna di Orbetello: studi, ricerche, criteri e modalità di intervento in quattrl anni di gestione commissariale 2003-2006. Presidenza del consiglio dei ministri, commissario delegato al risanamento ambientale della laguna di Orbtello.
Cappietti, L., Solari, S., Simonetti, I., Crema, I., 2020. Numerical modelling of Orbetello lagoon circulation in the XVIII century. In: IMEKO TC-19 International Workshop on Metrology for the Sea. IEEE, pp. 172–178.
Carvalho, R.C., Oliver, T.S., Woodroffe, C.D., 2019. Transition from marine to fluvial-dominated sediment supply at Shoalhaven prograded barrier, southeastern Australia. Geomorphology 341, 65–78.
Cattaneo, A., Steel, R.J., 2003. Transgressive deposits: a review of their variability. Earth Sci. Rev. 62, 187–228.
Chapkanski, S., Jacq, K., Brocard, G., Vittori, C., Debret, M., DeGiorgi, A., D'Ottavio, D., Giuffré, E.M., 2021. Calibration of short-wave infrared (SWIR) hyperspectral imaging using diffuse reflectance infrared Fourier Transform spectroscopy (DRIFTS) to obtain continuous logging of mineral abundances along sediment cores. Sedimentary Geology, 428, 106062.
Chapkanski, S., Brocard, G., Lavigne, F., Meilianda, E., Ismail, N., Darusman, D., Goiran, J.-P., 2022. Fingerprinting sources of beach sands by grain-size, using mid-infrared spectroscopy (MIRS) and portable XRF. Implications for coastal recovery along a tsunami-struck delta coastline. Catena 219, 106639.
Cheng, H., Edwards, R.L., Shen, C.-C., Polyak, V.J., Asmerom, Y., Woodhead, J., Hellstrom, J., Wang, Y., Kong, X., Spötl, C., 2013. Improvements in 230Th dating, 230Th and 234U half-life values, and U–Th isotopic measurements by multi-collector inductively coupled plasma mass spectrometry. Earth Planet. Sci. Lett. 371, 82–91.
Chiocci, F.L., 2000. Depositional response to Quaternary fourth-order sea-level fluctuations on the Latium margin (Tyrrhenian Sea, Italy). Geol. Soc. Lond. Spec. Publ. 172, 271–289.
Ciarletta, D.J., Shawler, J.L., Tenebruso, C., Hein, C.J., Lorenzo-Trueba, J., 2019. Reconstructing coastal sediment budgets from beach-and foredune-ridge morphology: a coupled field and modeling approach. J. Geophys. Res. Earth 124, 1398–1416.
Ciarletta, D.J., Miselis, J.L., Shawler, J.L., Hein, C.J., 2020. Quantifying thresholds of barrier geomorphic change in a cross-shore sediment partitioning model. Earth Surf. Dyn. Discuss. 2020, 1–36.
Cioffi, F., Gallerano, F., 2001. Management strategies for the control of eutrophication processes in Fogliano lagoon (Italy): a long-term analysis using a mathematical model. Appl. Math. Model. 25, 385–426.

Coltorti, M., Ravani, S., 2017. Caratteri geomorfologici della fascia costiera compresa tra la foce del fiume Albegna, la laguna di Orbetello e Ansedonia. Centro Studi di Preistoria e Archeoologia Milano, Italy, pp. 27–34.
Cooper, J., Jackson, D., Dawson, A., Dawson, S., Bates, C.R., Ritchie, W., 2012. Barrier islands on bedrock: a new landform type demonstrating the role of antecedent topography on barrier form and evolution. Geology 40, 923–926.
Cooper, J.A.G., Green, A.N., Loureiro, C., 2018. Geological constraints on mesoscale coastal barrier behaviour. Glob. Planet. Chang. 168, 15–34.
Cutroneo, L., Ferretti, G., Scafidi, D., Ardizzone, G.D., Vagge, G., Capello, M., 2017. Current observations from a looking down vertical V-ADCP: interaction with winds and tide? The case of Giglio Island (Tyrrhenian Sea, Italy). Oceanologia 59, 139–152.
De Giorgi, A.U., 2023. Old frameworks and new data. Orbetello, Cosa, and the making of the colony. In: Millet, M., Launaro, A. (Eds.), Roman Urbanism: Recent Discoveries and New Directions. Oxbow, Oxford, pp. 63–80.
Dillenburg, S.R., Hesp, P.A., Keane, R., da Silva, G.M., Sawakuchi, A.O., Moffat, I., Barboza, E.G., Bitencourt, V.J., 2020. Geochronology and evolution of a complex barrier, Younghusband Peninsula, South Australia. Geomorphology 354, 107044.
Dolci, M., 2014. Paesaggi d'Acque. In: Survey della laguna di Orbetello e del Monte Argentario. LANX. Rivista della Scuola di Specializzazione in Beni Archeologici-Università degli Studi di Milano, pp. 24–31.
Dolfini, A., 2017. La laguna nel tempo: stabilità e trasformazione del territorio: neolitico, eneolitco ed eta del bronto. In: Negroni Catacchio, N., Cardosa, M., Dolfini, A. (Eds.), Paesaggi d'acque: la Laguna di Orbetello e il Monte Argentario tra Preistoria ed Età Romana: un progetto di archeologia dei paesaggi dell'Università degli studi di Milano e del Centro studi di preistoria e archeologia di Milano, 2000-2006. Centro studi di preistoria e archeologia, pp. 310–327.
D'Orefice, M., Bellotti, P., Bertini, A., Calderoni, G., Censi Neri, P., Di Bella, L., Fiorenza, D., Foresi, L.M., Louvari, M.A., Rainone, L., 2020. Holocene evolution of the Burano Paleo-Lagoon (Southern Tuscany, Italy). Water 12, 1007.
D'Orefice, M., Bellotti, P., Bellotti, T., Davoli, L., Di Bella, L., 2022. Natural and cultural lost landscape during the Holocene along the Central Tyrrhenian Coast (Italy). Land 11, 344 s Note: MDPI stays neutral with regard to jurisdictional claims in published ….
Farquhar, O., 1967. Stages in island linking. Oceanogr. Mar. Biol. Annu. 5, 119–139.
Ferrarin, C., Roland, A., Bajo, M., Umgiesser, G., Cucco, A., Davolio, S., Buzzi, A., Malguzzi, P., Drofa, O., 2013. Tide-surge-wave modelling and forecasting in the Mediterranean Sea with focus on the Italian coast. Ocean Model 61, 38–48.
Ferri, S., Pranzini, E., 2006. Evoluzione del litorale dei tomboli della Giannella e di Feniglia, La Laguna di Orbetello: studi, ricerche, criteri e modalità di intervento in quattro anni di gestione commissariale 2003–2006. ColorDeSoli, Follonica, Grosseto, Tuscany.
Field, M.E., Roy, P.S., 1984. Offshore transport and sand-body formation; evidence from a steep, high-energy shoreface, southeastern Australia. J. Sediment. Res. 54, 1292–1302.
Flinn, D., 1997. The role of wave diffraction in the formation of St. Ninian's Ayre (Tombolo) in Shetland, Scotland. J. Coast. Res. 202–208.
Flores, R.P., Rijnsburger, S., Meirelles, S., Horner-Devine, A.R., Souza, A.J., Pietrzak, J. D., Henriquez, M., Reniers, A., 2018. Wave generation of gravity-driven sediment flows on a predominantly sandy seabed. Geophys. Res. Lett. 45, 7634–7645.
Fraccascia, S., Chiocci, F., Scrocca, D., Falese, F., 2013. Very high-resolution seismic stratigraphy of Pleistocene eustatic minima markers as a tool to reconstruct the tectonic evolution of the northern Latium shelf (Tyrrhenian Sea, Italy). Geology 41, 375–378.
Franz, G., Delpey, M.T., Brito, D., Pinto, L., Leitão, P., Neves, R., 2017. Modelling of sediment transport and morphological evolution under the combined action of waves and currents. Ocean Sci. 13, 673–690.
Funiciello, R., de Rita, D., Sposato, A., Esposito, A., Fabbri, M., Marsili, P., Mazzini, I., Paccara, P., Trigari, A., La Monica, G., 2020. Note Illustrative della Carta Geologica d'Italia alla scala 1: 50.000, Foglio 353 Montalto di Castro. APAT-Dipartimento Difesa del Suolo-Servizio Geologico d'Italia, Roma.
Galbraith, R.F., Roberts, R.G., 2012. Statistical aspects of equivalent dose and error calculation and display in OSL dating: an overview and some recommendations. Quat. Geochronol. 11, 1–27.
Garrison Jr., J.R., Williams, J., Potter Miller, S., Weber, E.T., McMechan, G., Zeng, X., 2010. Ground-penetrating radar study of North Padre Island: implications for barrier island internal architecture, model for growth of progradational microtidal barrier islands, and Gulf of Mexico sea-level cyclicity. J. Sediment. Res. 80, 303–319.
Gisotti, G., Lembo, P., 1992. La recente evoluzione del Tombolo di Feniglia e le sue cause. Boll. Soc. Geol. Ital. 111, 199–216.
González-Villanueva, R., Pérez-Arlucea, M., Alejo, I., Goble, R., 2009. Climatic-related factors controlling the sedimentary architecture of a barrier-lagoon complex in the context of the Holocene transgression. J. Coast. Res. 627–631.
Gosseaume, E., 1973. Le tombolo triple d'Orbetello (Toscane). Bulletin de la Société Languedocienne de Géographie 7, 3–11.
Heaton, T.J., Köhler, P., Butzin, M., Bard, E., Reimer, R.W., Austin, W.E., Ramsey, C.B., Grootes, P.M., Hughen, K.A., Kromer, B., 2020. Marine20—the marine radiocarbon age calibration curve (0–55,000 cal BP). Radiocarbon 62, 779–820.
Hsu, J.R., Silvester, R., 1990. Accretion behind single offshore breakwater. J. Waterw. Port Coast. Ocean Eng. 116, 362–380.
Huntley, D.J., Baril, M., 1997. The K content of the K-feldspars being measured in optical dating or in thermoluminescence dating. Ancient TL 15, 11–13.
Immenhauser, A., 2009. Estimating palaeo-water depth from the physical rock record. Earth Sci. Rev. 96, 107–139.
Jaffey, A., Flynn, K., Glendenin, L., Bentley, W.T., Essling, A., 1971. Precision measurement of half-lives and specific activities of U 235 and U 238. Phys. Rev. C 4, 1889.
Kinsela, M.A., Daley, M.J., Cowell, P.J., 2016. Origins of Holocene coastal strandplains in Southeast Australia: shoreface sand supply driven by disequilibrium morphology. Mar. Geol. 374, 14–30.
Klein, A.H.D.F., Junior, N.A., de Menezes, J.T., 2002. Shoreline salients and tombolos on the Santa Catarina coast (Brazil): description and analysis of the morphological relationships. J. Coast. Res. 425–440.
Knight, J., Burningham, H., 2022. A morphological classification of coastal forelands, with examples from South Africa. Geomorphology 415, 108410.
Lenzi, M., Palmieri, R., Porrello, S., 2003. Restoration of the eutrophic Orbetello lagoon (Tyrrhenian Sea, Italy): water quality management. Mar. Pollut. Bull. 46, 1540–1548.
Leoni, G., Dai Pra, G., 1997. Variazioni del livello del mare nel tardo olocene lungo la costa del lazio in base ad indicatori geo-archeologici. ENEA 115.
Li, B., Li, S.-H., 2011. Luminescence dating of K-feldspar from sediments: a protocol without anomalous fading correction. Quat. Geochronol. 6, 468–479.
Mazzini, I., Anadon, P., Barbieri, M., Castorina, F., Ferreli, L., Gliozzi, E., Mola, M., Vittori, E., 1999. Late Quaternary sea-level changes along the Tyrrhenian coast near Orbetello (Tuscany, Central Italy): palaeoenvironmental reconstruction using ostracods. Mar. Micropaleontol. 37, 289–311.
McCann, A.M., 2017. The Roman Port and Fishery of Cosa: A Center of Ancient Trade. Princeton University Press.
MEDAR_Group, 2002. MEDATLAS: mediterranean and black sea database of temperature, salinity and bio-chemical parameters and climatological atlas. In: SISMER, C.D.B (Ed.), 4 Cd-Roms, and Internet Server. www.ifremer.fr/sismer/program/medarIFREMER/TMSI/IDM/.
Michetti, L.M., 2017. Harbors. In: Naso, A. (Ed.), Etruscology. De Gruyter, Boston, Berlin, pp. 391–406.
Murray, A.S., Wintle, A.G., 2000. Luminescence dating of quartz using an improved single-aliquot regenerative-dose protocol. Radiat. Meas. 32, 57–73.
Negroni Catacchio, N., Cardosa, M., Dolfini, A., 2017. Ricostruire il paesaggio antico, Paesaggi d'Acque. In: La Laguna di Orbetello e il Monte Argentario tra Preistoria ed Eta Romana. Centro Studi di Preistoria e Archeologia Milano, pp. 372–384.
Negroni Catacchio, N., Cardosa, M., Rossi, F., 2019. Duna feniglia (Orbetello, GR). Un insediamento produttivo dell'età del ferro. Bolletino di Archeologia Online X, 51–66.
Nisi, M.F., Antonioli, F., Pra, G.D., Leoni, G., Silenzi, S., 2003. Coastal deformation between the Versilia and the Garigliano plains (Italy) since the last interglacial stage. J. Quat. Sci. 18, 709–721.
Oliver, T.S., Donaldson, P., Sharples, C., Roach, M., Woodroffe, C.D., 2017. Punctuated progradation of the seven mile beach Holocene barrier system, southeastern Tasmania. Mar. Geol. 386, 76–87.
Oliver, T.S., Murray-Wallace, C.V., Woodroffe, C.D., 2020. Holocene shoreline progradation and coastal evolution at Guichen and Rivoli Bays, southern Australia. The Holocene 30, 106–124.
Otvos, E.G., 2020. Coastal barriers-fresh look at origins, nomenclature and classification issues. Geomorphology 355, 107000.
Pasquetti, F., Vaselli, O., Zanchetta, G., Nisi, B., Lezzerini, M., Bini, M., Mele, D., 2020. Sedimentological, mineralogical and geochemical features of late Quaternary sediment profiles from the southern Tuscany Hg mercury district (Italy): evidence for the presence of pre-industrial mercury and arsenic concentrations. Water 12, 1998.
Pemberton, S.G., MacEachern, J.A., Dashtgard, S.E., Bann, K.L., Gingras, M.K., Zonneveld, J.-P., 2012. Shorefaces. In: Developments in Sedimentology. Elsevier, pp. 563–603.
Perkins, P., 2010. The Cultural and Political Landscape of the Ager Caletranus, North-West of Vulci. L'Antiquité Classique, Louvain-la-Neuve, pp. 103–121.
Pincherle, M., Volpi, G.C., 1989. Il porto invisibile di Orbetello. Pacini.
Poesini, S., 2012. La produzione ceramica di Punta degli Stretti (Orbetello, GR): aggiornamento degli studi. In: L'Etruria dal Paleolitico al Primo Ferro. Stato delle ricerche. Atti X, pp. 553–566.
Pons-Branchu, E., Douville, E., Dumont, E., Branchu, P., Thil, F., Frank, N., Bordier, L., Borst, W., 2014. Cross-dating (U/Th and lamina counting) of modern carbonate deposits in underground Paris, France. A new archive for urban history re-constructions: case study of anthropic rare Earth and Yttrium release. Quat. Geochronol. 24, 44–53.
Pons-Branchu, E., Barbarand, J., Caffy, I., Dapoigny, A., Drugat, L., Dumoulin, J., Alcaide, M.M., Nouet, J., Torti, J.S., Tisnérat-Laborde, N., 2022. U-series and radiocarbon cross dating of speleothems from Nerja Cave (Spain): evidence of open system behavior. Implication for the Spanish rock art chronology. Quat. Sci. Rev. 290, 107634.
Pranzini, E., Cinelli, I., Cipriani, L.E., Anfuso, G., 2020. An integrated coastal sediment management plan: the example of the Tuscany region (Italy). J. Mar. Sci. Eng. 8, 33.
Prescott, J.R., Hutton, J.T., 1994. Cosmic ray contributions to dose rates for luminescence and ESR dating: large depths and long-term time variations. Radiat. Meas. 23, 497–500.
Psuty, N., 2008. The coastal foredune: a morphological basis for regional coastal dune development. In: Coastal Dunes: Ecology and Conservation. Springer, pp. 11–27.
Reimer, P., McCormac, F., 2002. Marine radiocarbon reservoir corrections for the Mediterranean and Aegean Seas. Radiocarbon 44, 159–166.
Reimer, P.J., Austin, W.E., Bard, E., Bayliss, A., Blackwell, P.G., Ramsey, C.B., Butzin, M., Cheng, H., Edwards, R.L., Friedrich, M., 2020. The IntCal20 Northern Hemisphere radiocarbon age calibration curve (0–55 cal kBP). Radiocarbon 62, 725–757.
Richter, D., Richter, A., Dornich, K., 2013. Lexsyg—a new system for luminescence research. Geochronometria 40, 220–228.
Ridente, D., Petrungaro, R., Falese, F., Chiocci, F.L., 2012. Middle–Upper Pleistocene record of 100-ka depositional cycles on the Southern Tuscany continental margin (Tyrrhenian Sea, Italy): sequence architecture and margin growth pattern. Mar. Geol. 326, 1–13.

Rosa, M.L.C.D.C., Barboza, E.G., Abreu, V.D.S., Tomazelli, L.J., Dillenburg, S.R., 2017. High-frequency sequences in the Quaternary of Pelotas Basin (coastal plain): a record of degradational stacking as a function of longer-term base-level fall. Braz. J. Geol. 47, 183–207.
Rosati, J.D., Dean, R.G., Walton, T.L., 2013. The modified Bruun Rule extended for landward transport. Mar. Geol. 340, 71–81.
Rossi, F., 2017. Duna Feniglia–Sede Forestale (sito TF01). Un sito produttivo villanoviano. In: Paesaggi d'Acque La Laguna di Orbetello e il Monte Argentario tra Preistoria ed Età Romana. Milano, pp. 230–251.
Rossi, F., Campo, L., Cappello, I., Cardosa, M., Lepri, A., Luciano, M., 2014. Duna Feniglia (Orbetello, GR). I risultati delle ultime campagne di scavo (2011−2012) nell'area nord-occidentale. In: PPE Atti XI, pp. 681–688.
Roy, K., Peltier, W.R., 2018. Relative sea level in the Western Mediterranean basin: a regional test of the ICE-7G_NA (VM7) model and a constraint on late Holocene Antarctic deglaciation. Quat. Sci. Rev. 183, 76–87.
Roy, P., Thom, B., Wright, L., 1980. Holocene sequences on an embayed high-energy coast: an evolutionary model. Sediment. Geol. 26, 1–19.
Ryan, W.B., Carbotte, S.M., Coplan, J.O., O'Hara, S., Melkonian, A., Arko, R., Weissel, R. A., Ferrini, V., Goodwillie, A., Nitsche, F., Bonczkowski, J., 2009. Global multi-resolution topography synthesis. Geochemistry, Geophysics, Geosystems 10 (3).
Sabatier, P., Dezileau, L., Blanchemanche, P., Siani, G., Condomines, M., Bentaleb, I., Piquès, G., 2010. Holocene variations of radiocarbon reservoir ages in a Mediterranean lagoonal system. Radiocarbon 52, 91–102.
Sanderson, P.G., Eliot, I., 1996. Shoreline salients, cuspate forelands and tombolos on the coast of Western Australia. J. Coast. Res. 761–773.
Schmiedt, G., 1972. Il livello antico del Mar Tirreno: testimonianze dei resti archeologici. Olschki, Firenze.
Schulze, T., Schwahn, L., Fülling, A., Zeeden, C., Preusser, F., Sprafke, T., 2022. Investigating the loess–palaeosol sequence of Bahlingen-Schönenberg (Kaiserstuhl), southwestern Germany, using a multi-methodological approach. E&G Quat. Sci. J. 71, 145–162.
Schwahn, L., Schulze, T., Fülling, A., Zeeden, C., Preusser, F., Sprafke, T., 2023. Multi-method study of the Middle Pleistocene loess–palaeosol sequence of Köndringen, SW Germany. E&G Quat. Sci. J. 72, 1–21.
Shawler, J.L., Ciarletta, D.J., Connell, J.E., Boggs, B.Q., Lorenzo-Trueba, J., Hein, C.J., 2021. Relative influence of antecedent topography and sea-level rise on barrier-island migration. Sedimentology 68, 639–669.
Stive, M.J., De Vriend, H.J., 1995. Modelling shoreface profile evolution. Mar. Geol. 126, 235–248.
Sunamura, T., Mizuno, O., 1987. A study on depositional shoreline forms behind an island. In: Annual report of the Institute of Geoscience, 13. the University of Tsukuba, pp. 71–73.
Thom, B., 1984. Transgressive and regressive stratigraphies of coastal sand barriers in Southeast Australia. Mar. Geol. 56, 137–158.
Tortora, P., 1989. La sedimentazione olocenica nella plataforma continentale interna tra il promontoria di monte Argentario e la foce del fiume Mignone (Tirreno centrale). Giorn. Geol. 51, 93–117.
Tortora, P., 1996a. Depositional and erosional coastal processes during the last postglacial sea-level rise; an example from the central Tyrrhenian continental shelf (Italy). J. Sediment. Res. 66, 391–405.
Tortora, P., 1996b. Utilizzazione di carte granulometriche vettoriali nelle indagini sulla provenienza e dispersione del sedimento: un esempio dal fondale ad est del promontorio di Monte Argentario (piattaforma toscana). Boll. Soc. Geol. Ital. 115, 219–240.
Tsuguo, S., 1987. A study on depositional shoreline forms behind an island. In: Annual report of the Institute of Geoscience, 13. the University of Tsukuba, pp. 71–73.
Vacchi, M., Marriner, N., Morhange, C., Spada, G., Fontana, A., Rovere, A., 2016. Multiproxy assessment of Holocene relative sea-level changes in the western Mediterranean: sea-level variability and improvements in the definition of the isostatic signal. Earth Sci. Rev. 155, 172–197.
Vella, C., Lippmann-Provansal, M., Long, L., Bourcier, M., 2000. Contexte géomorphologique de trois ports antiques provençaux: Fos, Les Laurons, Olbia. Méditerranée 94, 39–46.
Vetrano, A., Napolitano, E., Iacono, R., Schroeder, K., Gasparini, G.P., 2010. Tyrrhenian sea circulation and water mass fluxes in spring 2004: observations and model results. J. Geophys. Res. Oceans 115.
Waelbroeck, C., Labeyrie, L., Michel, E., Duplessy, J.-C., Mcmanus, J.F., Lambeck, K., Balbon, E., Labracherie, M., 2002. Sea-level and deep water temperature changes derived from benthic foraminifera isotopic records. Quat. Sci. Rev. 21, 295–305.
Wohlfarth, B., 2013. A review of early Weichselian climate (MIS 5d-a) in Europe. In: Technical report/Svensk kärnbränslehantering AB, p. 44.
Zecchin, M., Catuneanu, O., Caffau, M., 2019. Wave-ravinement surfaces: classification and key characteristics. Earth Sci. Rev. 188, 210–239.
Zoppi, U., Albani, A., Ammerman, A., Hua, Q., Lawson, E., Barbero, R.S., 2001. Preliminary estimate of the reservoir age in the lagoon of Venice. Radiocarbon 43, 489–494.